THE EXCITATION OF TURBULENCE IN SEPARATED LAMINAR BOUNDARY LAYERS

P. Freymuth

Translation of "Über die Anfachung von Störungen in abgelösten laminaren Grenzschichten," Deutsche Luft-und Raumfahrt, Report DLR-FB 66-02, January 1966, pp. 1-63.

NATIONAL AERONAUTICS AND SPACE ADMINISTRATION
WASHINGTON, D. C. 20546 APRIL 1972

TABLE OF CONTENTS

1. Notation

1.	$w = (x, y, z)$	Position vector
2.	θ	Pulse loss thickness in a free jet
3.	θ_0	Pulse loss thickness at the edge of the nozzle
4.	θ_m	Pulse loss thickness at a distance of $x_m/D = 0.026$ and $x_m/h = 0.045$ from the nozzle edge
5.	δ^*	Displacement thickness
6.	d_1, d_2, d_3	Distances of maxima occurring in amplitude variations from the principal maximum
7.	D	Diameter of spin effect nozzle
8.	h	Channel width of flat nozzle
9.	$\vec{w} = (U+u, v, 0)$	Velocity vector
10.	U_0	Velocity of free jet in the core of the jet
11.	a_s	Speed of sound
12.	$\hat{c}_1, \hat{c}_2, \hat{c}_3$	Amplitude of maxima occurring in the amplitude variations
13.	Ω	Vorticity for two-dimensional flow
14.	f	Sound frequency
15.	t	Time
16.	p	Pressure
17.	p_0	Standard pressure
18.	P	Pressure of sound
19.	P_s	pressure of sound on the boundary in speaker vicinity
20.	$P_{stau} = \rho_0 U_0^2/2$	Dynamic pressure
21.	ρ	Density
22.	ρ_0	Standard density
23.	$\nu = 0.15\ cm^2\ sec^{-1}$	Kinematic viscosity of air
24.	Γ_{krit}	Critical circulation according to a hypothesis of time
25.	$M = U_0/a_s$	Mach number
26.	$S = f \cdot \theta_m/U_0$	Strouhal number

27.	$Re = U_o \cdot \theta_m/\nu$ $Re_D = U_o \cdot D/\nu$ $Re_h = U_o \cdot h/\nu$	Reynolds numbers
28.	$a' = \alpha_i \theta_m$	Dimensionless excitation factor
29.	$-\alpha_i$	Excitation factor
30.	Ψ	Complex flow function
31.	$\Phi = \Phi_r + i\Phi_i$	Eigen function to determine the flow function
32.	ϵ	Small number

THE EXCITATION OF TURBULENCE IN SEPARATED LAMINAR BOUNDARY LAYERS

P. Freymuth[1]

ABSTRACT: This paper deals with the growth of turbulence in separated laminar boundary layers as a function of the hydrodynamic characteristic numbers for high Reynolds numbers. The experiments show that only the Strouhal number has an effect on the spatially growing disturbances. Thus, the basic equations of the process become simple. The theoretical results are in good agreement with the experiments.

2. Introduction

/7*

Laminar, stationary flow configurations with rotation frequently tend to become periodic in a nonstationary manner and finally irregular. This involves the well-known transition from laminar to turbulent flow, which had been investigated first by Reynolds [1] on the example of pipe flow. Since then, a voluminous literature concerned with the problem of the excitation of small turbulences has been created. Among the best known are the solution for the Prandtl plate boundary layer by Tollmine [2] and Schlichting [3]. The range of transition from exponentially excited, periodic disturbance to fully turbulent motion, on the other hand, has not yet found a uniform solution. In the field of the wall boundary layer there exists Gortler's theory [4] of secondary instability with longitudinal vortices, which recently has been confirmed by experiments. For separated boundary layers, e.g., the initially laminar boundary layer accompanying free jets, Wille [5] and Domm [6] developed a concept. According to them, the transition of excited waves to full turbulence is shown to consist of a periodic sequence of annular vortices. The latter decompose three-dimensionally and form the start of turbulence. The concept was confirmed by Wille et al. in free shear layers exiting from nozzles [7, 8, 9, 10, 11]. Work

---

1. German Research Institute for Aerospace Flight, Research Report No. 66-02, January 1966. Dissertation approved by the Department of Machine Design, Berlin Technical University.

* Numbers in the margin indicate pagination in the foreign text.

performed within the program of the DVL Institute for Turbulence Research concerning laminar-turbulent transitions resulted, however, in a series of detail problems which proved to be difficult to solve.

1. The cause of the decomposition of the vortices formed remained unexplained. Timme [12] formulated a hypothesis, applied by Fabian [13] to the mixing zone of a free jet, which assumes a critical Reynolds number Γ_{krit}/ν. After this number has been reached, the vortices decompose. Friction is assumed to play a substantial part in the mechanism of vortex decomposition. A paper by Domm [6] involves centrifugal forces in an explanation of vortice instability. Both hypotheses, however, do not lend themselves to close examination.

2. Due to the undetermined dependence of small turbulence introduced to the (e.g., by sound) some of Wille's [8] experimental results concerning the excitation of turbulence in separated boundary layer remain unclear. Thus, at constant sound pressure, excitation depended on flow velocity, which remains to be explained. In addition, there were differences in the generation of turbulence with a speaker or a vibrating strip which rendered the evaluation of measured results difficult.

3. Extensive calculations by Michalke and Schade [14, 15, 16] concerning /8
the excitation of turbulence in free boundary layers in part did not result in convincing agreement with the experiments, or else no adequate measurements were available to confirm the theory. Thus, measured results to determine the dependence of excitation on the frequency of turbulences were insufficient for a comparison with theory. Fabian [13] noted in his experimental work concerning the excitation of turbulence that during the passage through the boundary layer with a hot wire probe, a 180° phase shift of the turbulence excited occurred. This phenomenon has been noted previously by Sato [17] in his work on the excitation of turbulence in separated boundary layers. The theory of wavelike excitation of Michalke and Schade does not yield such a phase shift. The fundamental principles of their theory thus appear to be unconfirmed. For this reason, Timme and Fabian attempted to explain the phase shift by the existence of vortices.

4. While, however, vortex model representations with wake flow yielded good agreement with experiments [12, 18], the method failed when applied to free shear layers.

5. Due to intensive research with methods of the hot wire technique, little attention was paid to smoke patterns. The explanation of hot wire signals by vortices therefore remained hypothetical [5, 6]. The present paper is intended as a contribution to the clarification of the problems outlined above. It is based on the multitude of stimulating hypotheses and experimental experiences accumulated since 1952 in the Institute for Turbulence Research.

3. Theoretical Foundations and Experimental Problem /9

The paper investigates the laminar-turbulent transition in free shear layers exiting from round or planar nozzles under the effect of sound. Under the influence of sound the shear layer begins to wave is rolled meanderingly into vortices which finally decompose in a turbulent manner, as shown in Figure 1.

The problem initially depends on a disturbing number of parameters which make a solution of the problems mentioned in Chapter 2 difficult. The following parameters must be considered: position coordinates, time, nozzle geometry, acoustic pressure, sound frequency, jet velocity, geometry of the acoustic field, boundary layer thickness, turbulence of flow from the nozzle, turbulence noise.

Due to the number of parameters, the present work began with the question of the conditions under which boundary layer flows of the type under consideration are dynamically similar. One begins with the hydrodynamic fundamental equations and the given boundary conditions.

The fundamental equations are:

$$\frac{\partial \mathfrak{w}}{\partial t} + \mathfrak{w} \cdot \operatorname{grad} \mathfrak{w} = -\frac{\operatorname{grad} p}{\rho} + \nu \Delta \mathfrak{w} \tag{1}$$

$$-\frac{\partial \rho}{\partial t} = \operatorname{div} \rho \mathfrak{w} \tag{2}$$

$$p - p_0 = c^2 (\rho - \rho_0) \tag{3}$$

In Eq. (1), mass forces (gravity) and the compression component of friction were neglected. Since the main stream of the free jet leaving the nozzle is isothermal, barotropy was assumed in Eq. (3); in addition, pressure and density variations due to the acoustic effect were assumed to be small.

The boundary conditions:

(4.1) $U = U(y)$, given that it rises from zero velocity over the boundary layer with a pulse loss thickness θ_0 to the jet velocity U_0.

In addition, in the vicinity of the speaker the acoustic pressure is given: /10

$$P_s = P_{sr} \sin 2\pi ft \tag{4.2}$$

By introducing dimensionless variables, the fundamental equations and boundary conditions can be made dimensionless with characteristic values of the problem:

$$t = \frac{\Theta}{U_0} t' \qquad \Delta r = \Theta \Delta r' \qquad \Delta w = U_0 \Delta w' \tag{5}$$

$$\rho = \rho_0 \rho' \qquad p = p_0 + \rho_0 U_0^2 p'$$

Substitution of Eq. (5) in Eq. (1) and rewriting with the following abbreviations yields: $\frac{f\Theta}{U_0} = S$ $\qquad \frac{U_0 \Theta}{\nu} = Re$ $\qquad \frac{U_0}{a_s} = M$

$$\frac{\partial \Delta w'}{\partial t'} + \Delta w' \operatorname{grad}' \Delta w' = -\frac{\operatorname{grad} p'}{\rho'} + \frac{1}{Re} \Delta' \Delta w' \tag{1a}$$

Substitution of Eq. (5) in Eq. (2) yields:

$$\frac{-\partial \rho'}{\partial t'} = \operatorname{div}' \rho' w' \tag{2a}$$

Substitution of Eq. (5) in Eq. (3) yields:

$$\rho' = 1 + M^2 p' \tag{3a}$$

Substitution of Eq. (5) in Eq. (4.2) yields:

$$P_s' = \frac{P_s}{\rho_0 U_0^2} \sin 2\pi St' = \frac{P_s}{2P_{stau}} \sin 2\pi St' \tag{4.2a}$$

Eqs. (1a) to (4.2a) contain the following characteristic numbers:

1. S — Strouhal number
2. Re — Reynolds number
3. M — Mach number
4. P_s/P_{stau} — Ratio of acoustic pressure to dynamic pressure.

To this, in principle (5), the degree of turbulence of the stream leaving the nozzle and (6), the turbulence noise level in relation to the sound level, are added. Since they represent troublesome interference values, they were

largely suppressed in the experiments and were neglected in the initial theoretical statement.

In practice, one is far removed from a solution of the system of Eqs. (1a) /11
to (4a). It thus became necessary to determine the dependence of excitation on the characteristic numbers 1 to 4 experimentally, in the hope that the results justify simplifications in the system of equations.

4. Experimental Apparatus and Methods

The experiments were performed on a free jet produced in a free-jet device. Turbulence was excited in the boundary layer with a loudspeaker; its excitation was examined by the hot wire measuring technique. The experiments were intended to determine the dependence of the turbulence excitation on the characteristic numbers 1 - 4. Since velocity variations measured with the hot wire apparatus contained harmonics in an undeterminable manner, only the fundamental wave of the turbulence excited was evaluated with a narrow-band frequency analyzer.

In order to visualize the results as much as possible, they were correlated with a "vortex pattern" obtained from smoke patterns of the turbulent flow.

Measuring instruments and methods are described in greater detail in the following subchapters.

4.1. Free jet device

An existing installation of the DVL Institute for Turbulence Research was utilized to produce the free jet; it has been described in [8]. The installation consists of a fan to generate the pressure necessary to produce the jet. It is followed by a large attenuation chamber to quiet the air moved by the fan; the latter then enters the measuring room through a nozzle as a free jet. The wind channel and the measuring room is surrounded with acoustically insulated walls to reduce the interference noise level. In order to keep the fan noise from the jet, acoustic dampers were built in between the fan and the attenuation chamber. /12
A high rpm radial fan with blades bent backwards was used; it showed little pressure variation in operation.

Michalke's [19] rotation-symmetrical vortex thread nozzles, used in previous investigations, were employed as the exit nozzles for the free jet, as well as a flat nozzle with a circular arc contour, as shown in Figure 2. Great care was taken to create favorable inlet conditions into the nozzle. The sharp-edged

inner border of the vortice thread nozzles was eliminated by a foam rubber wall, as shown in Figure 3. Velocity variations in the boundary layer were reduced in this manner. Presumably, irregular boundary layer separations occurred at the edge. Figure 4 shows velocity profiles directly behind the edge of the nozzle. The nozzle was mounted on an aluminum plate which was connected rigidly with the attenuation chamber. The turbulence variations which took place under the effect of the slightest vibrations in earlier measurements were thus eliminated.

4.2. Hot wire measuring technique

Flow velocity and its variation in time were measured with a hot wire apparatus according to Berger, Freymuth, Froebel [20]. The hot wire apparatus was located on a measuring stand outside the measuring room, as shown in Figure 5, while the hot wire probe was mounted directly in front of the free jet nozzle on a support (Figure 6). With the aid of two synchronous motor drives, the probe could be moved in the direction of the jet and perpendicularly to it through the boundary layer. The position of the probe was communicated by way of an electric relay to the measuring stand in 0.2-mm intervals.

A voltage is linearly coordinated with the flow velocity at the location of the hot wire by way of the linearization stage of the hot wire apparatus; the potential is communicated to a galvanometer loop of the scanning recorder (Visicorder, Honeywell). It is also connected with a narrow-band frequency analyzer (Rhode and Schwarz, Type FTA). For the purpose of phase measurements, the potential is amplified over a narrow band and transmitted to a phase meter (Rhode and Schwarz, Type PZN).

Sound for excitation of turbulence in the boundary layer was produced by a speaker, mounted above the nozzle, or as shown in Figure 3, inside the attenuation chamber in front of the nozzle. /13 The speaker is powered by an on-line generator of the frequency analyzer. The sound and analyzer frequencies are always coordinated with each other. The analyzer provides a direct current voltage proportional to the fundamental wave, which powers another galvanometer loop of the scanning recorder.

The hot wire signal may be viewed on an oscilloscope and also the voltage of the microphone which measures the acoustic pressure. Figure 7 presents the block diagram of the measuring arrangement.

4.3. Smoke signal technique

To supplement results obtained with the hot wire technique, smoke patterns were recorded with stroboscope illumination and correlated with the hot wire analyses. The following concept makes an interpretation of smoke patterns possible.

In a two-dimensional frictionless liquid the vorticity is

$$d\Omega/dt = 0.$$

Vorticity is thus attached to the substance. If a substance of a certain vorticity is colored with smoke, an image of the distribution of the vorticity in the excited boundary layer is obtained. This therefore yields a method for the measurement of rotation which provides an insight in the flow mechanism. As will be shown in Chapter 5.2.3, the condition of freedom of friction is approximately satisfied.

The smoke was blown with the aid of a slight stream of air from a smoke tubelet of the Auer Company into the boundary layer at the lower edge of the nozzle. The "vortex pattern" was stroboscopically illuminated and sometimes photographed. In addition, during the observation of the vortex patterns analyses of the disturbances were conducted by the hot wire technique and visually coordinated with the vortex pattern.

4.4. Measuring methods

/14

4.4.1. Determination of pulse loss thickness

In earlier work in the institute, the displacement thickness δ^* was chosen as a characteristic length [8]. But δ^* is defined only at the nozzle wall and is difficult to determine, because while measuring in the nozzle there is always the danger of destroying the hot wire. There exists, however, a more important reason to select another characteristic length which is also defined in the free jet: the excitation is embedded in the velocity profile and not in the wall boundary layer of the nozzle. The momentum loss thickness θ in the free jet was selected.

It is defined by:

$$\theta = \int_{-\infty}^{\infty} u/U_o\,(1-u/U_o)\,dy \qquad (6)$$

In practice, the integral must be extended over the range of the shear layer. The dependence of θ on the length of path x may be represented within the context of the boundary layer theory in the following form.

1. For a round nozzle:

$$\theta/D\sqrt{Re_D} = f_1(x/D) \tag{7}$$

It follows for $\theta_0 = \theta(x = 0)$:

$$\theta_0/D\sqrt{Re_D} = \text{const} \tag{8}$$

It follows from Eqs. (7) and (8):

$$\theta/\theta_0 = f(x/D) \tag{9}$$

2. For a flat nozzle:

$$\theta/h\sqrt{Re_h} = g_1(x/h) \tag{7a}$$

$$\theta/h\sqrt{Re_h} = \text{const} \tag{8a}$$

$$\theta/\theta_0 = g(x/h) \tag{9a}$$

The constants in Eqs. (8) and (8a) and the dependence on the length of path were determined experimentally. For this purpose, the velocity profiles were traversed by the hot wire probe at different distances from the edge of the nozzle and recorded with the Visicorder (Figure 11), the function $\frac{u}{U_0}\left(1 - \frac{u}{U_0}\right)$ calculated (Figure 8) and determined by graphical integration θ. As the characteristic length, not θ_0 but a somewhat different value θ_m was chosen; this will be justified in Chapter 5.1. /15

4.4.2. Analysis of turbulence excited

While the velocity of the free jet, the frequency of the sound and its intensity remain constant, the hot wire probe is passed transversely through the boundary layer and the hot wire signal and the analyzer indication, designated in the following as amplitude variation are recorded automatically with the scanning recorder. By including the interval marking points (all Δ y = 0.2 mm) the y scale in the measuring diagram is established. Figure 11b shows, e.g., a

diagram obtained in this manner. In the amplitude variation two maxima with a minimum between them may be recognized, but up to three maxima may appear, as shown in Figure 11c.

The dependence of excitation on the length of path was determined by repeating the process described above with different x values.

Experimental investigations with the hot wire measuring technique were concentrated on the recording and evaluation of amplitude variations, but phase variations were also determined.

By varying the hydrodynamic characteristic values, their effect on the flow process was clarified and important knowledge for a theoretical treatment of the problem was found.

5. Experimental Results

5.1. Momentum loss thickness

Figure 9 shows the dependence of θ/θ_0 on the length of path, recorded at U_0 = 8 m/sec for round and flat nozzles.

For θ_0:

$$\theta_0/D\sqrt{Re_D} = 0.53 \qquad (15)$$

correspondingly:

$$\theta_0/h\sqrt{Re_h} = 0.68$$

Figure 10a-c presents some of the velocity profiles on which evaluations were based. Figure 9 indicates a moderate dependence of θ/θ_0 on the length of path in the vicinity of the edge of the nozzle, which declines rapidly. Within this range, the transformation of the unsymmetrical wall boundary layer profile of the free shear layer takes place, as shown in Figure 10c. Since the initiation was investigated thoroughly only in the area of the fully formed free shear layer (details in Chapter 6.1), the value of θ will be taken arbitrarily but justifiably, as the characteristic length at a location

$$x_m/D = 0.026 \quad (x_m = 10\,\theta_0 \text{ for } U_0 = 8 \text{ m/s} \quad D = 7.5 \text{ cm})$$

or

$$x_m/h = 0.045 \quad (x_m = 10\,\theta_0 \text{ for } U_0 = 8 \text{ m/s} \text{ flat nozzle})$$

On the one hand, at x_m one is still in the vicinity of the nozzle edge, and on the other hand, the value is representative in the range of the fully formed shear layer also, because θ varies only slightly for $x > x_m$. For θ_m, in accordance with Eqs. (8) and (8a):

$$\theta_m/D\sqrt{Re_D} = 0.61$$

$$\theta_m/h\sqrt{Re_h} = 0.82$$

5.2. Results of the excitation analyses

Prior to the reporting of the evaluation of the measured results in detail, a general description of the development of amplitude variations with the length of path will be given, because roughly the same pattern was obtained regardless of the choice of characteristic values.

Directly at the mouth of the nozzle an amplitude maximum was found when traversing the velocity profile; this maximum may be attributed directly to the acoustic effect, which is shown in Figure 11a and has not been evaluated (details in Chapters 6.1 and 8.1). As shown in Figure 11b[1], somewhat farther down /17

1. For small disturbance amplitudes another peaking of the larger maximum occurs in the amplitude variation (Figure 12). The cause of this effect is not hydrodynamic, as shown by an investigation, but is to be found in the linearization of the hot wire signal by a diode circuit. In order to obtain a potential proportional to the velocity from the hot wire apparatus, during the passage through the boundary layer different sensitivities are established by switching the diodes on or off, for the evaluation of the hot wire signal [20]. At each inclusion or exclusion of a new diode a change in sensitivity occurs, which becomes particularly noticeable in the analysis of small velocity variations. To confirm this, the speed of sound in a nozzle stream was analyzed; a slow decline of velocity was achieved by turning off the fan. In this case again the switching off of diodes with declining velocities must be noticeable in the analysis. The result of the analysis and the decline of velocity were recorded by a scanner. The result was Figure 13. It is seen that the switching off of a diode with declining velocities results in an abrupt reduction in sensitivity, followed by an increase in sensitivity due to King's law. In the case of very low velocities, sensitivity collapses, because of the reduction of heat transfer from the hot wire at high acoustic frequencies and low flow velocities. In the evaluation of amplitude variations of the turbulence excited, the fine structure was bypassed by graphical interpolation, due to the mechanism described above.

the stream the fluctuations became such that two maxima with a minimum between them occur. This pattern is being maintained over a considerable length of path with merely the maxima growing larger. Finally, however, a third maximum emerges, Figure 11c, which farther down merges with the principal maximum (Figure 11d). Still farther down the stream, the recording becomes too disturbed for an evaluation (Figure 11e), and the flow becomes turbulent.

The characteristic fluctuation maxima $\hat{c}_{1,2,3}/U_0$ and the correlated distances from the principal maximum $d_{1,2,3}/U_0$ in accordance with Figure 11c were evaluated as a function of the length of path x/θ_m. The maxima were plotted logarithmically.

In order to obtain the dependence of the resulting curves on flow characteristics, one of these was varied in each case, while the others were held constant or varied only if their negligibility has been proven. The families of characteristic curves obtained in this manner are represented graphically.

5.2.1. Dependence of excitation $\hat{c}_2/U_0$ on P_s/P_{stau}

Because of its simplicity, the dependence of excitation on the acoustic pressure will be treated first.

In Figure 14, the dependence of the principal maximum $\hat{c}_2/U_0$ on the length of path x/θ_m is plotted logarithmically for different acoustic pressures. Velocity U_0 and the acoustic frequency f were held constant. A vortex thread nozzle with a diameter of 7.5 cm was used.

It is seen that the curves differ only by a shift and that they may be represented over a large part of the path by a straight line. In addition, the curves are at an equal distance from each other. One may therefore write the following for the straight-line portion of the curves:

$$c_2/U_0 \sim P_s/P_{stau}\, e^{a' \cdot x/\theta_m} \qquad (10)$$

Velocity variations first increase exponentially and are directly proportional to the acoustic pressure. They finally attain a maximum, decline slightly and cannot be evaluated later, because a merger of the principal maximum with the third maximum takes place.

5.2.2. Dependence of excitation $\hat{c}_2/U_0$ on the Mach number

In Figure 15, the excitation $\hat{c}_2/U_0$ was represented as a function of P_s/P_{stau} at a constant Stroubal number. In this case, however, P_s/P_{stau} was varied by changing U_0 and making P_s proportional to U_0: /19

$$\frac{P_s}{P_{stau}} \sim \frac{U_0}{\frac{\rho}{2} U_0^2} \sim \frac{1}{U_0}$$

The acoustic frequency was chosen so that the same Strouhal number S = 0.0118 was obtained which is in agreement with the Strouhal number of turbulence excited without sound (see Chapter 8.2). The equidistance of the curves again yields Eq. (10). Since the Mach number varies with varying values of P_s/P_{stau} without affecting the resulting Eq. (10), it was concluded that the problem does not depend on the Mach number.

Figure 15 indicates that the characteristic number P_s/P_{stau} produces merely a displacement of the excitation curve and is thus involved only in the initiation but not in the development of the excitation process in the boundary layer. By introducing a standardized zero point, therefore, a uniform representation of excitation ration curves may be obtained. The point at which $\hat{c}_2/U_0$ has the value of 0.0025 on the abscissa has been designated the zero point. All of the excitation curves displayed up to now then coincide within the limits of measuring accuracy. This is independent of the position of the speaker.

5.2.3. Dependence of excitation on the Reynolds number

Figure 16 shows the dependence of $\hat{c}_1/U_0$ and $\hat{c}_2/U_0$ on the Reynolds number Re_D for vortex thread nozzles. Figure 17 indicates this dependence for $\hat{c}_3/U_0$. Figure 18 displays the coordinated distances $d_{1,2,3}/\theta_m$ from the principal minimum.

The variation of the Reynolds number was achieved by varying the velocity (U_0 = 2 - 32 m/sec) and by selecting different nozzle diameters (D = 7.5 cm; 10 cm; 14 cm).

It is seen that within an accuracy of ±10% there is no appreciable frictional effect. Excitation thus does not depend substantially on friction.

5.2.4. Dependence of excitation on the Strouhal number /20

It is seen in Chapters 5.2.1 - 5.2.3 that there are no Mach number effects, that the dependence of the pressure ratio P_s/P_{stau} can be eliminated by introducing a standard zero point and that the Reynolds number is not essential, i.e., that friction may be neglected. It remains to determine the dependence of turbulence excitation on the Strouhal number.

Excitation curves were established at constant velocity for different Strouhal numbers. Strouhal numbers were varied by changing the frequency of sound. Figures 19-21 exhibit the dependence of the excitation curves $\hat{c}_{1,2,3}/U_o$ of the Strouhal number, Figures 22-24 the correlated $d_{1,2,3}/\theta_m$ distances from the principal maximum for a vortex thread nozzle. As a supplement, in Figure 25 the excitation curves $\hat{c}_2/U_o$ are plotted for a flat nozzle.

Figures 19-21 indicate that with growing Strouhal numbers maxima $\hat{c}_1$ and $\hat{c}_3$ are becoming gradually more pronounced than $\hat{c}_2$. In Figure 26, the $\hat{c}_1/\hat{c}_2$ ratio is displayed to visualize the effect for the linear range of excitation. The ratio increases with growing Strouhal numbers.

Figures 22-24 indicate that the geometric dimensions of turbulent flow decrease with increasing Strouhal numbers. As in Figure 18, it is seen in Figures 22 and 23 that the geometric dimensions of turbulent flow do not depend on the length of path for small values of x/θ_m.

Round and flat nozzles yield roughly the same results, i.e., in both cases a characteristic length, the momentum loss thickness θ_m, suffices for the characterization. The nozzle diameter D or the channel width h do not enter the result. Measurements of the wave number also yield the same results for round and flat nozzles, as shown in Figure 27. The theoretical curves, also shown, will be discussed in Chapter 7.

5.2.5. Phase measurements

As a supplement to the analyses of fundamental wave amplitudes, phase variations were also measured. Qualitatively, there are no differences for different Strouhal numbers. Since no quantitative evaluation of the phase measurements was performed, Figure 28 should suffice. Consideration of phase variations while /21 passing through the boundary layer from the outside inward yields the following findings. Initially the phase varies hardly at all, until an abrupt phase change

occurs at the minimum of fluctuations at about 180°. During the rest of the passage there is constant change in the phase.

5.3. Correlation of smoke patterns in excitation analysis

As indicated in Chapter 4.3, smoke patterns provide an excellent view of vorticity distribution.

Figure 29 exhibits the process of vortex roll-up with sound excitation ($S = 0.0118$; $U_0 = 3$ m/sec). In each sectional image there was a 60° phase rotation with respect to the preceding. Smoke was introduced through a smoke pipe at the lower edge of the boundary layer.

A slightly wavy range may be observed in the vicinity of the nozzle which is followed by turbulent flow[2]. Simultaneous observation of the smoke pattern and hot wire analysis yielded a correlation as shown in Figure 30.

The most important result of the correlation is the fact that in the wavy range of excitation two maxima already appear with a minimum between them in amplitude variation and that the abrupt phase change is also developed at the location of the minimum. It is therefore less than meaningful to explain this excitation configuration by vortices.

Hot wire analyses always yield a highly unsymmetrical impression. It was therefore assumed that this lack of symmetry will also appear in the smoke patterns. As seen in Figure 31, this is only true conditionally. Unsymmetrical appearances such as shown in Figure 32, for example, can be compensated for by placing an outline of Figure 31 over it in the manner done in Figure 32. Here the smoke is blown into a higher layer of the stream. Unsymmetrical smoke patterns can be complemented to a certain degree, antisymmetrically, by another pattern obtained at a different height of the boundary layer.

Figures 33a and 33b indicate that the geometrical dimensions of the vortices depend strongly on the Strouhal number; this was also the result of the hot wire analyses (Figure 22-24).

Figure 33c shows that in the case of excessive Strouhal numbers the turbulence excitation due to sound excitation is masked by the natural excitation. /22

2. For an explanation of the use of the concepts of "wave" and "vortex" see Chapter 6.2.

The stroboscope was synchronized with the frequency of sound; two light flashes occurred during the exposure.

Figure 34 indicates an impression of the slippage of vortices which always took place and which found its expression in the hot wire signals by components of the fundamental frequency.

6. Interpretation of Experimental Results

6.1. The four ranges of excitation

The experimental results of Chapter 5 suggests a division into four ranges of turbulence excitation; these are of great usefulness for the theoretical understanding of the exciting mechanism (Figure 30).

Excitation begins in the vicinity of the nozzle edge, where turbulences are forced by sound pressure. Amplitude variation shows only a single maximum. In this range, turbulences are transformed in the form necessary for exponential excitation with two maxima in the amplitude variation. This range is therefore designated the transformation range.

Somewhat farther downstream, excitation reaches the stage of a wave excited linearly at a logarithmic scale[3]. Two maxima occur in the amplitude variation.

The range of linear excitation is followed by the range of nonlinear excitation, which in the smoke patterns is characterized by vortices. Initially, three maxima appear in the amplitude variation, of which the two larger ones merge into a single maximum downstream.

The ranges of linear and nonlinear excitation together form the range of laminar-turbulent transition. This is followed by the turbulent range in which an evaluation of amplitude variations is no longer possible.

The present work is concentrated on the range of laminar-turbulent transition /23 which is amenable to systematic investigations, as shown in Chapter 5. The transformation range, in which compressibility and friction certainly cannot be neglected, was not investigated in this series of experiments because the excitation structure existing in that range is not effective in the adjacent ranges. The present work owes its consequent feasibility to this fact.

---

3. This range may be described by the linearized stability theory which, as is known, yields exponentially excited solutions [24].

In the transformation range, in addition to the transformation of the structure of turbulence, the transformation of the wall boundary layer profile into the free shear layer profile also takes place. Processes in the transformation range are thus extremely complex and therefore difficult to interpret theoretically.

6.2. Waves and vortices

In the preceding chapters the concepts of "wave" and "vortex" were used without presenting a definition of the concepts. Since in general usage, the designations of waves and vortices are used ambiguously, it is necessary to define them clearly with respect to their application in the present paper. This, however, will be done only now, in order to include experimental experience.

In general linguistic use, "waves" represent a process and mixtures of processes that are periodic in time and space. Damped and excited processes and their mixtures are also designated as waves.

In general linguistic use, "vortices" means areas of a liquid in circular motion. Examples are the potential vortex and the Hamel-Oseen vortex. If several vortices are found in a periodic arrangement, one speaks of vortex roads which in their entirety again form a wave. For the purposes of the present work and in approximation of the vortex concept which emerges from the work of Timme [12] and Fabian [13], the definitions of "wave" and "vortex" will be much more restricted. Let the starting point of the definitions be the distribution of vorticity as indicated by smoke patterns (see Chapter 4.3). "Wave" thus represents a flow configuration with its vorticity arranged in the form of a slightly bent band which does not return onto itself. The concentration of vorticity along the band varies only slightly. Example: range 2 in Figure 30. /24

"Vortex" indicates a configuration with a vorticity strongly concentrated in comparison with its environment. A strong decline of this concentration must exist in all directions perpendicular to the axis of vorticity. Example: range 3b in Figure 30.

6.3. Reduction of fundamental equations

The experiments described in Chapter 5 were intended to clarify the conditions of a theoretical treatment of the problem under consideration. The fundamental equations were to be written as simply as possible.

In accordance with Chapters 5.2 and 5.3, the effect of sound remains restricted to the vicinity of the edge of the nozzle. It determines the initial turbulence from which the excitation takes its further development. This fact has been already anticipated by Brown [21] for the case of narrow slit nozzles.

Subsequently, the turbulences are excited exponentially, which leads to the conclusion that this particular range can be described by a linearized theory of stability [24]. As is known, this yields exponentially excited waves. The smoke patterns of Chapter 5.3 demonstrate the wave character in the linear excitation range. It is therefore not surprising that the vortex model concepts as developed by Timme and Fabian for the linear range met with little success.

Chapter 5.2.3 shows that the Reynolds number in the laminar-turbulent transition range has no significant effect. Friction is effective only within the nozzle in the formation of the wall boundary layer and in the transformation range in the development of the free shear layer. The assumption that the frictional effect is insignificant in the laminar-turbulent transition range represented the motivation for the present work. Since the experimental proof of independence of friction of the excitation process for $10^4 \leqq Re_D \leqq 3 \times 10^5$ represents one of the focal points of the work, three considerations which lead to the initiation of the experiments shall be discussed.

1. For large Reynolds numbers the friction term of the Navier-Stokes equation [Eq. (1)] becomes small. It may thus be neglected if no boundary conditions incompatible with the Euler equation, e.g., wall adhesion, are present. In free jets, such conditions do not exist. For sufficiently large Reynolds numbers, therefore, the friction effect must be negligible. /25

2. Earlier work at the institute already indicated that the effect of friction on the stability behavior of the boundary layer in the Reynolds number range under consideration is negligible [8, 9, 14, 15]. With increasing distances from the edge of the nozzle, however, the importance of friction increases rather than decreases, as shown by the following consideration. With growing lengths of path, vorticity is being concentrated and with it the surface surrounding the vorticity declines. This reduces the friction diffusion of vorticity ($d\Omega/dt = \nu \Delta \Omega$), i.e., the frictional effect decreases.

3. In the case of turbulent decomposition of vortices, the forces of turbulent momentum exchange far exceed the frictional forces. Thus, Bradshaw et

al. [22] found a value of 20 for the ratio of turbulent forces to frictional forces in a fully turbulent free jet at $Re_D = 10^4$.

It has been shown, among others, in Chapter 5.2 that only one characteristic length, e.g., θ_m can be correlated with the problems under consideration. Both planar and rotation-symmetrical problems can be described by the same (planar) statement.

The conclusions drawn from the experiments in the foregoing lead to a substantial simplification of fundamental equations and contain suggestions with respect to a theoretical treatment. In the following the reduced system of equations is written together with certain suggestions:

$$\frac{\partial w'}{\partial t'} + w' \cdot \operatorname{grad}' w' = -\operatorname{grad}' p' \qquad (1b)$$

$$\operatorname{div} w' = 0 \qquad (2b)$$

Eq. (3b) is eliminated. The problem is planar.

The profile of the fundamental flow is antisymmetrical.

For a substantial part of the length of path a linearized theory of the turbulences excited exponentially with x is adequate.

6.4. Conclusions derived from the reduced fundamental equations /26

6.4.1. Spatial excitation

The reduced fundamental equations and the experiments indicate that of the hydrodynamic characteristic numbers only the Strouhal number remains. Only because the experiments reduced the number of characteristic values through restriction to the laminar-turbulent transition range were they capable of producing clear results. The multiplicity of factors that must have expected otherwise could not have been handled.

The reduction of characteristic numbers yielded simplifications for the theory also, so that the theoretical treatment became possible.

The reduced system of equations shows that a spatial excitation problem exists. Calculations performed earlier by Michalke and Schade, used heretofore for the verification of experiments, extended, however, to excitation problems

in time only. Excitation in time was assumed to be related in a simple manner to excitation in space.

However, experiments described in Chapter 5.2 indicates clearly that in the linear range they cannot be described by the theory of excitation in time. In particular, the strong lack of symmetry of amplitude variations, the abrupt change in phase and their complex dependence on the Strouhal number, are incompatible with the theory of excitation in time. The latter requires amplitude variations symmetrical with respect to the center of profile and monotonous phase behavior. The phase jog has been observed earlier and lead to vortex model concepts by Timme and Fabian.

It was assumed that the cause of all these effects is the laminar boundary layer broadening due to friction. As shown in Chapter 5.1, however, the broadening of the jet in the excitation range under consideration is slight. Following the proof of the independence of the problem investigated from the Reynolds number (Chapter 5.2.3) and the voluminous investigations concerning its dependence on the Strouhal number, it became necessary to search for other causes for the failure of the theory.

A comparison of the reduced equations in Chapter 6.2 with the assumptions of the calculations by Michalke surprisingly showed that they differ only in the assumption of space or time excitation.

If no entirely unknown assumptions, also neglected in the reduced system of equations are responsible for the incorrect results of the earlier calculations, only the assumption of excitation in time could be taken as the cause. /27

The following analogy consideration suggests the hypothesis that the unsymmetrical development of turbulence excited is the result of spatial excitation. It is known that two-dimensional antisymmetrical boundary layers develop in an unsymmetrical manner under the effect of friction. The distribution of vorticity in such stationary friction-afflicted flows is described by the following equations:

$$\vec{AD} \cdot \operatorname{grad} \Omega = \nu \Delta \Omega$$

For excited, instationary flows free of friction, on the other hand, the following average value equation is valid

$$\bar{\vec{AD}} \cdot \operatorname{grad} \bar{\Omega} = \overline{\vec{AD} \cdot \operatorname{grad} \tilde{\Omega}}$$

The place of the friction term here is taken by the eddy viscosity. In the same manner as the vorticity is distributed unsymmetrically under the effect of friction it is distributed under the influence of eddy viscosity.

Originally it was intended merely to present a suggestion in the present work concerning the theoretical treatment of spatial excitation. In the meantime, however, it became possible to develop the theoretical considerations of spatial excitation by Michalke [23], through the utilization of his great experience in the calculation of time excitation, to the extent that, based on his investigations concerning the distribution of vorticity, the calculation of hot wire analyses became feasible. This calculation was performed by the author on an electronic computer and compared with the results. Details are reported in Chapter 7.

6.4.2. Causes of vortex dissociation

Since friction is negligible with respect to the turbulent flow under consideration, it cannot be used to explain the dissociation of vortices. The hypothesis of a critical circulation Γ_{krit}/ν, at which the vortices decompose had to be abandoned, therefore, for the case of the turbulent flow under consideration here at large Reynolds numbers $Re_D \geq 10^4$. /28

Rayleigh's criterion for centrifugal instability is also not satisfied, because this requires vorticities with positive and negative signs.

It is therefore presumed that the cause of vortex decomposition is the induction of vortices. The slipping of vortices, as shown in Figure 34, presents a clear image of their mutual induction. In addition, Figure 34 also shows vortex decomposition after slipping. It may thus be assumed that the mutual induction of vortices is responsible for their three-dimensional decomposition. Presumably, the induction effect of a vortex upon itself is of lesser importance, because experiments of single vortices indicated that they are of longer life. A final statement, however, cannot be made until detailed investigations of single vortices have been conducted.

7. Theory of Spatial Excitation and Comparison with Experimental Results

7.1. Linearized theory of spatial excitation

Based on the necessity of developing a theory of spatial excitation in order

to explain the experimental results of the present work, Michalke [23] succeeded in deriving a mathematical solution in analogy to the calculation of excitation in time [16].

Michalke's calculation was then used by the present author in the calculation of amplitude and phase variations of analyses obtained with hot wires. This theory, to the extent required, will be outlined in the following.

The theory begins with Rayleigh's stability equation for two-dimensional flow (see, e.g., [16], [24]):

$$(U(y)-c)\left(\frac{d^2\phi(y)}{dy^2}-\alpha^2\phi(y)\right)-\frac{d^2U(y)}{dy^2}\cdot\phi(y)=0$$

where

$U(y)$ is dimensionless velocity profile of undisturbed flow;

$\Phi(y)$ serves to determine the dimensionless flow function Ψ:

$$\Psi=\text{Realteil}(\phi e^{i\alpha(x-ct)})=\text{Re}(\phi e^{i(\alpha x-\omega t)}) \qquad /29$$

The dimensionless turbulence velocity components u and v may be determined from Ψ:

$$u=\epsilon\frac{\partial\Psi}{\partial y} \qquad v=\frac{\partial\Psi}{\partial x}$$

The theory is valid for sufficiently small values of ϵ.

The theory is executed for dimensionless values, which in this chapter, as an exception, are not identified by an apostrophe.

While for excitation in time c is taken as a complex number and α as a real number, [16, 24], in the case of spatial excitation ω must be real and α complex [23]:

$$\omega=2\pi S \qquad \alpha=\alpha_r+i\alpha_i$$

For the fundamental flow a hyperbolic tangent model was chosen; it must be antisymmetrical and is in good agreement with measured profile values in the range of laminar-turbulent transition, as shown in Figure 35.

$$U(y) = 0.5\,(1 + \tanh 0.5\,y)$$

The boundary condition is the same as in excitation in time:

$$\phi(-\infty) = \phi(\infty) = 0$$

As in the case of excitation with respect to time, for spatial excitation the eigenfunctions Φ_r and Φ_i for the determination of $\Phi = \Phi_r + i\Phi$ are obtained from the numerical integration of the Rayleigh equation performed by Michalke on an electronic computer (ZUSE 23). The eigen values α_r and α_i were also determined for several Strouhal numbers numerically. With α_r α_i Φ_r and Φ_i the flow function Ψ is defined.

Engineering professor Michalke has provided the present author with the subprograms for the determination of Φ_r, Φ_i and their derivation with respect to y for two different Strouhal numbers to calculate hot wire analyses. /30

The amplitude variation and the phase variation of the fundamental wave of the hot wire signals were calculated and compared with the experiments. The calculation was performed both for spatial and time excitation to clearly demonstrate the difference between the two modes of excitation.

For fluctuations c/U_0, measured with hot wires, the following is approximately valid:

$$\frac{c}{U_0} \approx u = \varepsilon\, \mathrm{Re}\left(\frac{\partial \psi_1}{\partial y}\right) \text{ with } \psi_1 = \phi e^{i(\alpha x - \omega t)}$$

$$\frac{\partial \psi_1}{\partial y} = \left(\frac{d\phi_r}{dy} + i\,\frac{d\phi_i}{dy}\right) \cdot e^{i\left[(\alpha_r + i\alpha_i)x - 2\pi S t\right]}$$

$$\frac{c}{U_0} = \varepsilon\, \mathrm{Re}\left(e^{-\alpha_i x} \sqrt{\left(\frac{d\phi_r}{dy}\right)^2 + \left(\frac{d\phi_i}{dy}\right)^2}\right) e^{i(\alpha_r x - 2\pi S t + \delta)}$$

$$\text{with } \sin\delta = \frac{\frac{d\phi_i}{dy}}{\sqrt{\left(\frac{d\phi_r}{dy}\right)^2 + \left(\frac{d\phi_i}{dy}\right)^2}}$$

It follows for amplitude c/U_0:

$$\frac{1}{\varepsilon e^{-\alpha_i x}} \cdot \frac{c}{U_0} = \sqrt{\left(\frac{d\phi_r}{dy}\right)^2 + \left(\frac{d\phi_i}{dy}\right)^2} \qquad \text{amplitude variation}$$

and for phase δ:

$$\delta = \arcsin \frac{\frac{d\phi_i}{dy}}{\sqrt{\left(\frac{d\phi_r}{dy}\right)^2 + \left(\frac{d\phi_i}{dy}\right)^2}} \qquad \text{phase variation}$$

Numerical results are presented in the following section and compared with the experiments.

7.2. Comparison of calculated and measured hot wire analyses

The amplitude and phase variation was calculated for two different Strouhal numbers in the range of exponential excitation (S = 0.008 and S = 0.017). In Figures 36 and 37 amplitude variation for S = 0.008 and S = 0.017 is represented in the form yielded by the spatial and time excitation mode. In addition, measured amplitude variations standardized with respect to the height of the principal maximum are also plotted. It is seen that for the smaller Strouhal number the theoretical curve for spatial excitation is in almost quantitative agreement with the experimental curve. For larger Strouhal numbers a difference results from the fact that here even in the case of the smallest length of path a third maximum occurs in the experiment. Presumably, this is due to a very early effect of the nonlinearity of excitation for large Strouhal numbers.

The excessively rapid decline of measured amplitude variations toward small flow velocities is probably due to a measuring error in the hot wire method. The method is not suited for the measurement of small flow fluctuations at high frequency (here 1770 Hz) with low fundamental flow velocities, because in such cases heat transfer from the hot wire is strongly reduced.

A comparison of theoretical amplitude variations for spatial excitation shows in accordance with Figure 36 and 37 that with rising Strouhal numbers the minimum migrates more toward the inside of the boundary layer, i.e., it is located at higher values of velocity. In addition, the ratio of the height of the small maximum to the height of the large maximum increases. Both results had been

determined experimentally and the variation plotted with the Strouhal number in Figures 27 and 38. In Figures 26 and 38, in addition to measured values, calculated curves are plotted. The measured values are in very good agreement with these curves.

In Figures 39 and 40, calculated phase variations for spatial and time excitation are plotted. The phase jump of spatial excitation at the location of the minimum in the amplitude variation is seen. The phase progress is approximately the same as the measured variation in Figure 28.

Another comparison of calculated and experimental values concern the dependence of the excitation factor, $-\alpha_i\theta_m$, on the Strouhal number. This de- /32
pendence was calculated by Michalke and is shown in Figure 41. In addition to the calculated curves for excitation in space and in time, the measured values obtained from the initial rise of the excitation curves $\hat{c}_2/U_0$ in Figures 20 and 25 are also shown. Good agreement of measured values with the curve of spatial excitation is obtained for $S < 0.012$. For higher Strouhal numbers agreement with the curve of excitation in time is better. The same is true for the comparison of the calculated and measured dependence of the wave number on the Strouhal number, as shown in Figure 27.

The moderate discrepancy between the theory of spatial excitation and measured results for large Strouhal numbers is presumably a consequence of the fact that the linearized theory is strictly valid for large Strouhal numbers only with very small disturbances. Turbulences excited in practice with the speaker were too large.

8. Appendix

Present State of Research in the Laminar-Turbulent Transition of a Separated Boundary Layer

Certain problems of laminar-turbulent transition were clarified in the present work. A review of some of the open problems on the periphery of the work is presented to supplement the image of the present state of research in laminar-turbulent transition in a separated shear layer.

8.1. The transition range

As mentioned in Chapter 6.1, the range of the excitation of turbulence in the vicinity of nozzle edges was not investigated in detail. This range, due to

the very small amplitude variations and the effect of compressibility, is nearer to the field of acoustics than to aerodynamics. In spite of small disturbance amplitudes, because of the structure of turbulences expressed in amplitude variations by a single maximum, the transition range cannot be described by the stability theory as developed to this date. Figure 42 demonstrates with the aid /33 of an example that no strictly exponential excitation occurs in the transition range. The nonexponential curves, such as those obtained through excitation with a vibrating band [8, 9], are also presumably due to the effect of transition. Turbulences produced by the vibrating band are neither small nor do they exhibit the structure of amplitude variation necessary according to the theory of exponential excitation.

8.2. Natural frequency

It is known from earlier measurements [8, 9] that the rolling up of boundary layers into vortices takes place even without the effect of sound. The "natural frequency" around which the rolling process cycles is correlated with a "natural Strouhal number" $S_{nat} = 0.0118$. Based on theories of spatial and time excitation, nothing can be said concerning the stabilization of the rollup process at the natural frequency. A weak reaction of the fully formed turbulent flow on the range of the nozzle edge is assumed. With a strong reaction, as in the case of vortex paths behind cylinders, a higher frequency constant would be expected. The assumption that the natural frequency is identical with the maximum excited frequency [8] could not be confirmed. The result was $S_{nat} = 0.0118$ and $S_{max} = 0.017$.

8.3. Laminar-turbulent transition with small Reynolds numbers

The present work was restricted to investigations at large Reynolds numbers in the range of the laminar-turbulent transition ($Re_D \geqq 10^4$; $Re_h \geqq 5300$), where frictional effects proved to be negligible. For substantially smaller Reynolds numbers the frictional effect must be significant. Investigations at small Reynolds numbers are planned for a later time when suitable apparatus is available. Even at very high Reynolds numbers a modification may occur through the fact that the range of profile transformation becomes very large.

8.4. Theory of nonlinear excitation and of vortex decomposition /34

The fundamental principles of a mathematical treatment of the excitation

problem under consideration were developed. Mathematical execution, however, initially was restricted to the linearized theory. The range of the fully formed turbulent flow, the slippage of vortices and their three-dimensional decomposition poses extensive mathematical demands. Solutions are feasible only by way of numerical methods with the aid of large computers.

The present work was performed at the VDL Institute for Turbulence Research, under the direction of Prof. Dr. R. Wille. I wish to express my thanks to him for his generous support and valuable advice during the course of the work.

The work has been based greatly on the scientific work of Wille and his co-workers Domm, Timme, Fabian, Michalke, Schade, and Berger, concerning laminar-turbulent transition which was communicated to me in many discussions by the scientists of the Institute for Turbulence Research and of the Hermann Fottinger Institute for Flow Technology. My thanks are due to them also. The author is grateful for his friendly acceptance in the community of the coworkers of both institutes.

Figure 1. Vortices colored with smoke in a separated nozzle boundary layer. U_o = 3 m/s; D = 7.5 cm; f = 95 Hz.

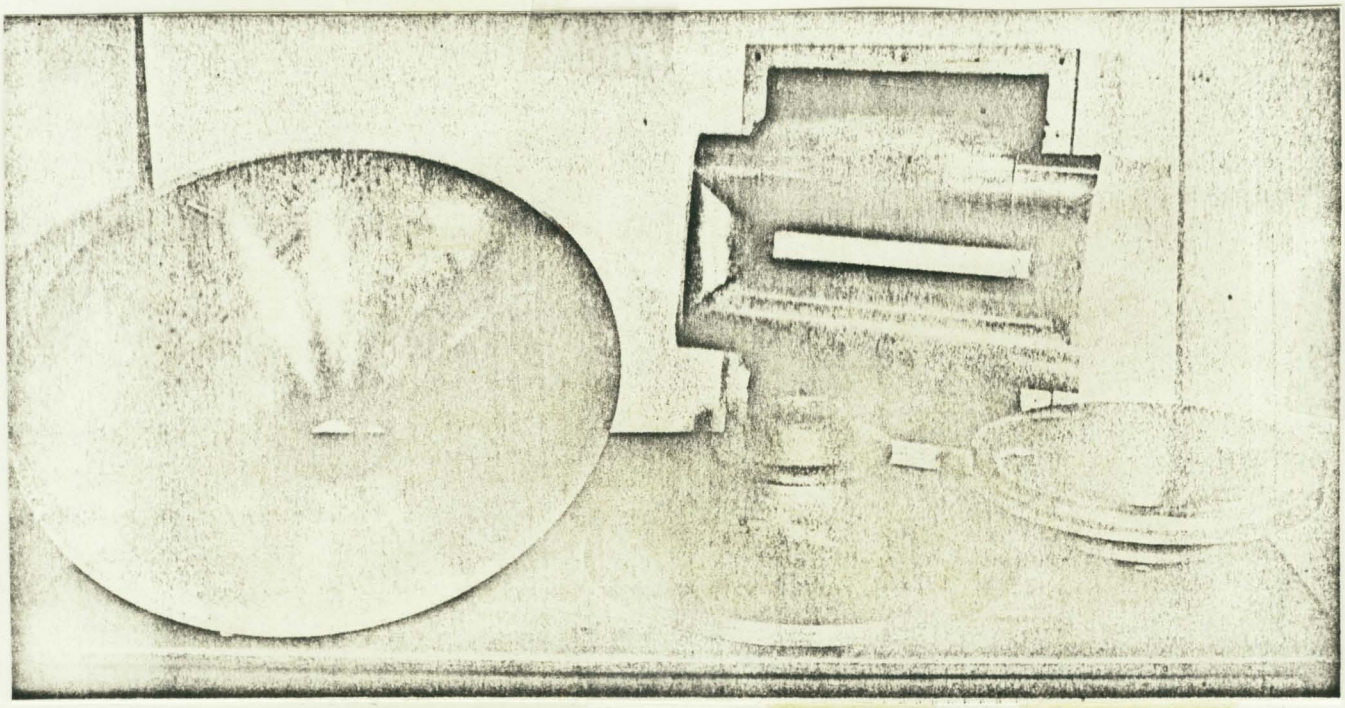

Figure 2. Vortex thread nozzles and flat nozzles.

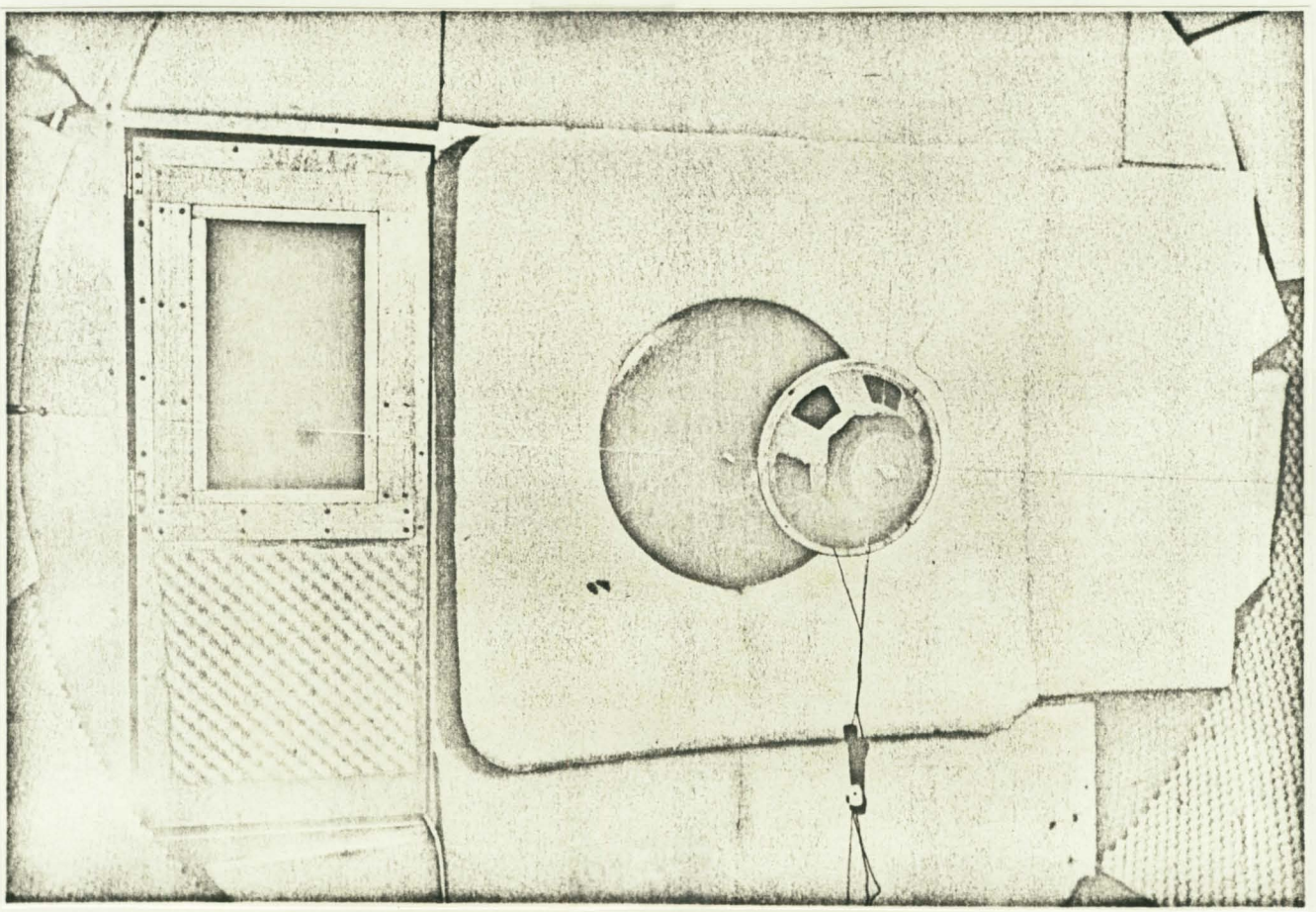

Figure 3. Round nozzle with foam rubber backing and speaker in front of the nozzle.

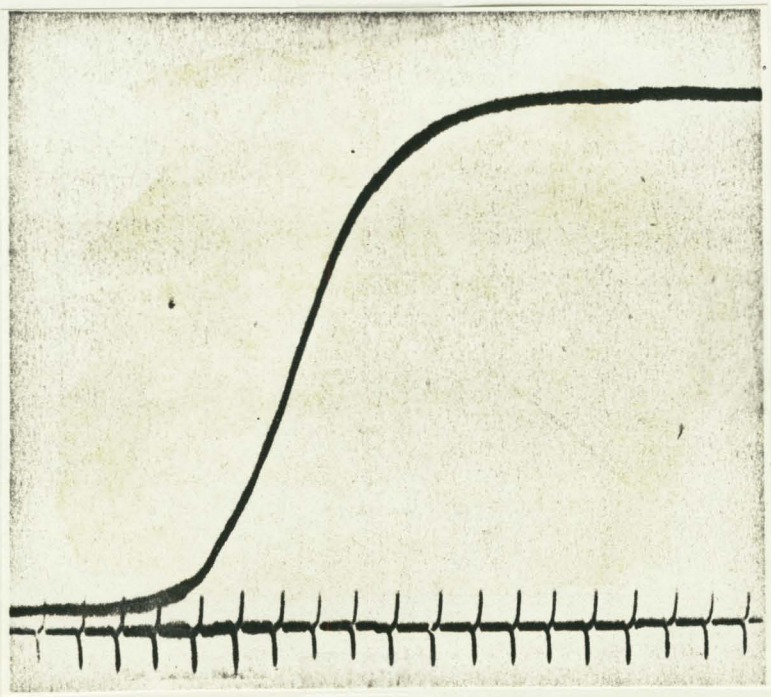

Figure 4a. Velocity profile in a free jet with foam rubber backing of the inner edge of the nozzle. U_o = 8 m/s; D = 7.5 cm.

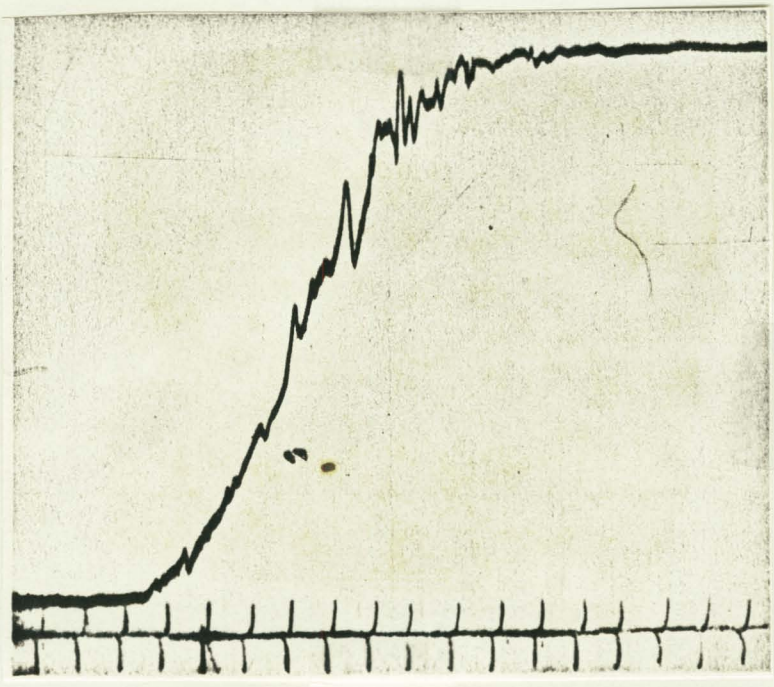

Figure 4b. Velocity profile in a free jet without foam rubber backing of the inner edge of the nozzle. U_o = 8 m/s; D = 7.5 cm.

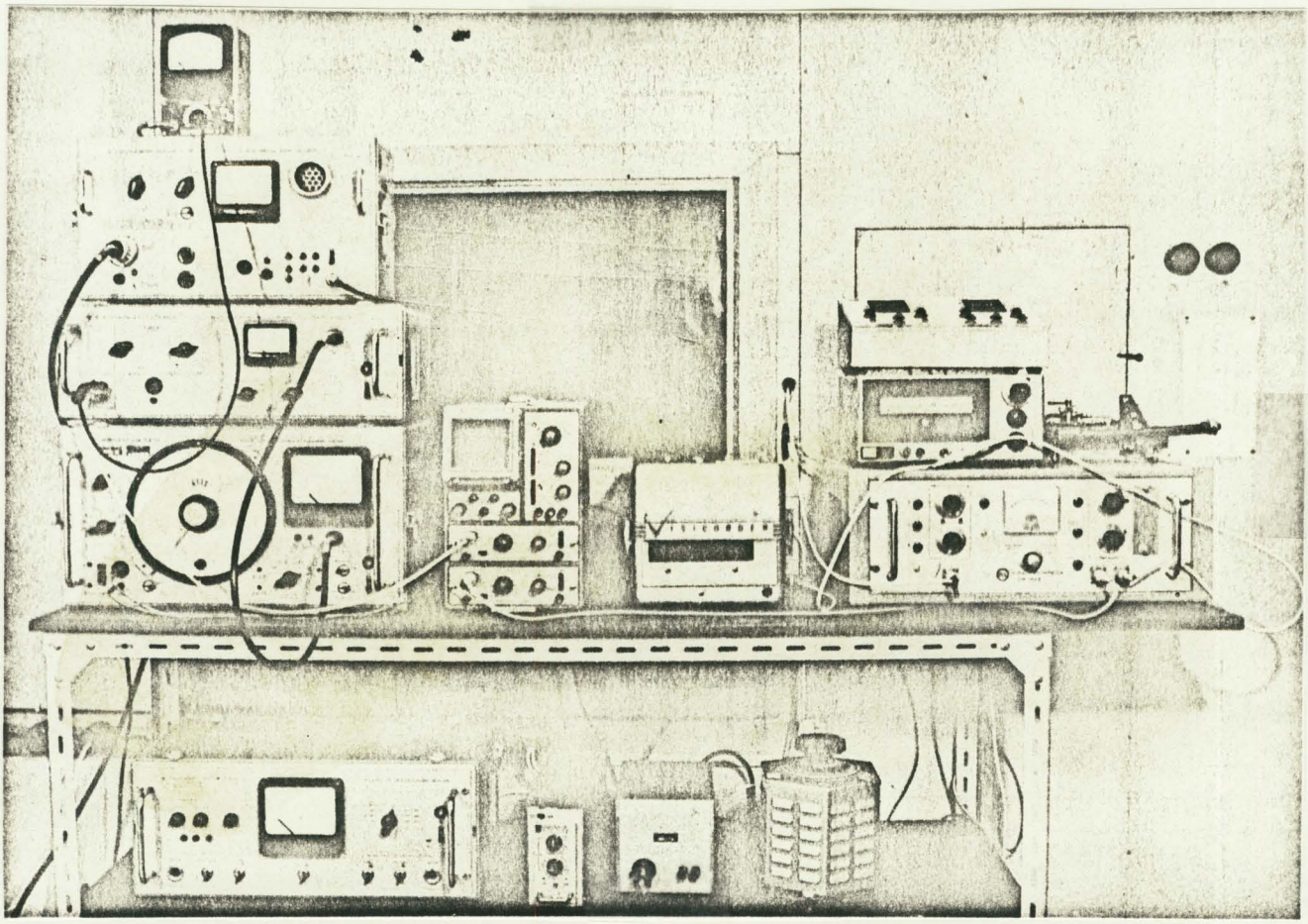

Figure 5. Measuring stand.

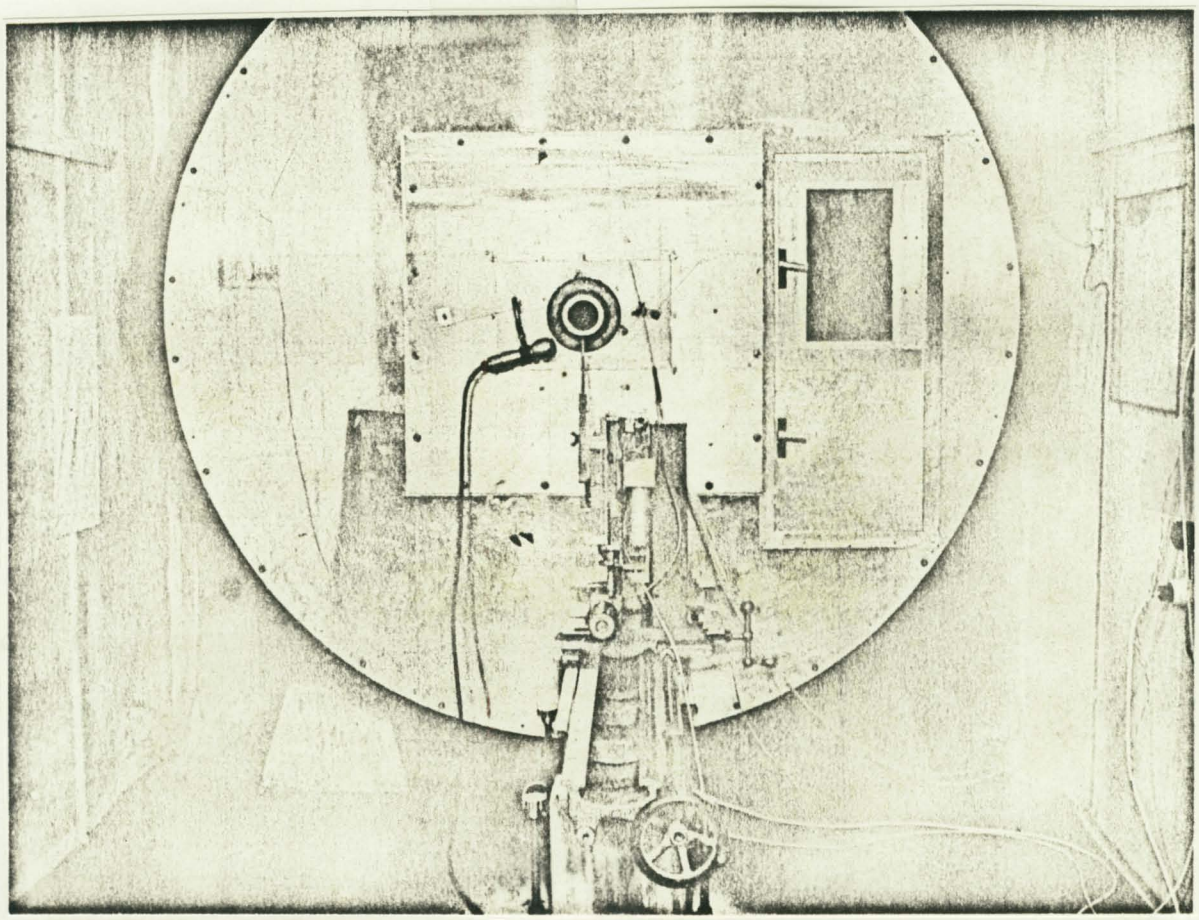

Figure 6. Measuring room.

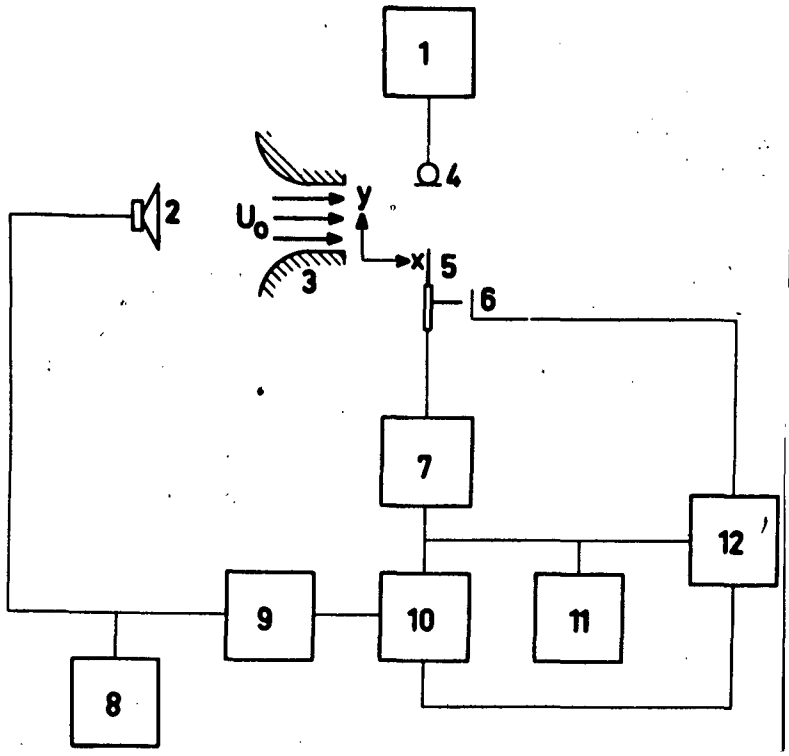

1. Sound level recorder
2. Speaker
3. Nozzle
4. Microphone
5. Hot wire probe
6. Path indicator
7. Hot wire apparatus
8. Frequency meter
9. On-line generator
10. Analyzer
11. Oscilloscope
12. Visicorder

Figure 7. Block diagram of measuring circuit.

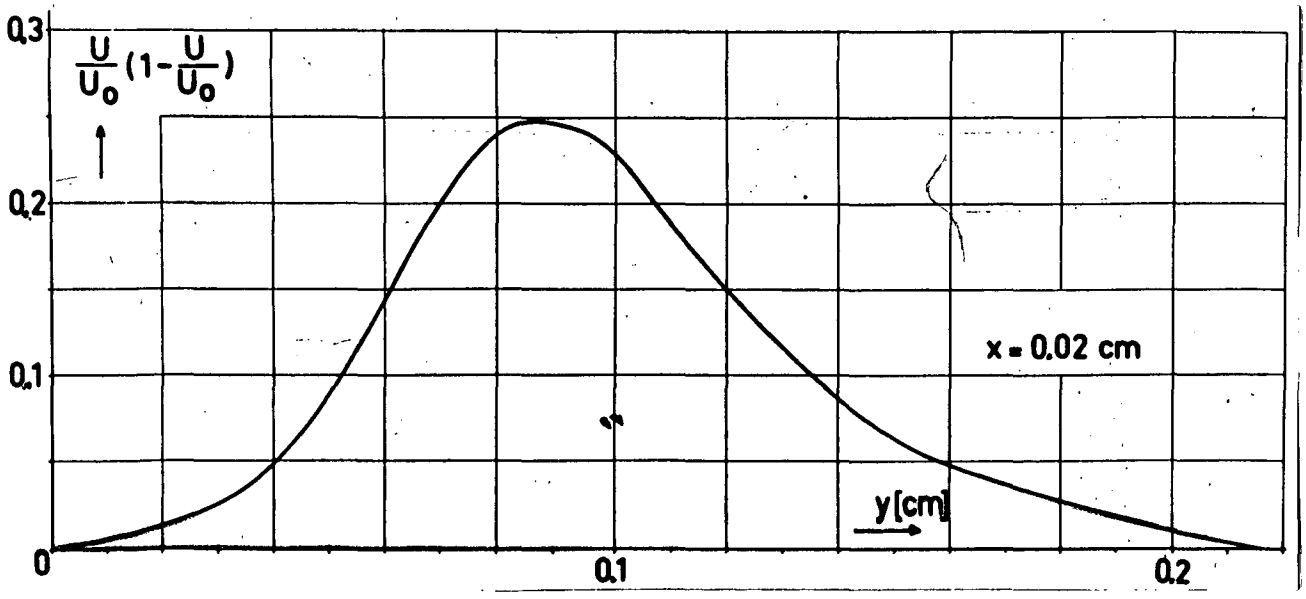

Figure 8. The $U/U_o(1 - U/U_o)$ function as a function of y.

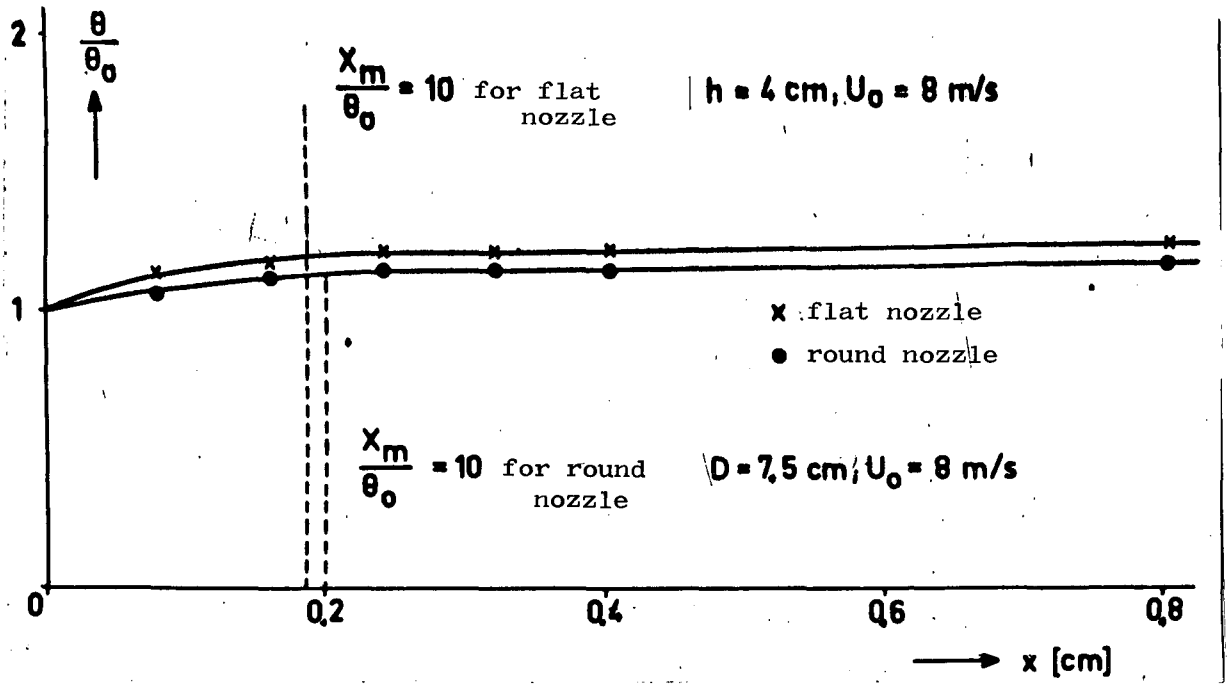

Figure 9. Momentum loss thickness θ as a function of length of path.

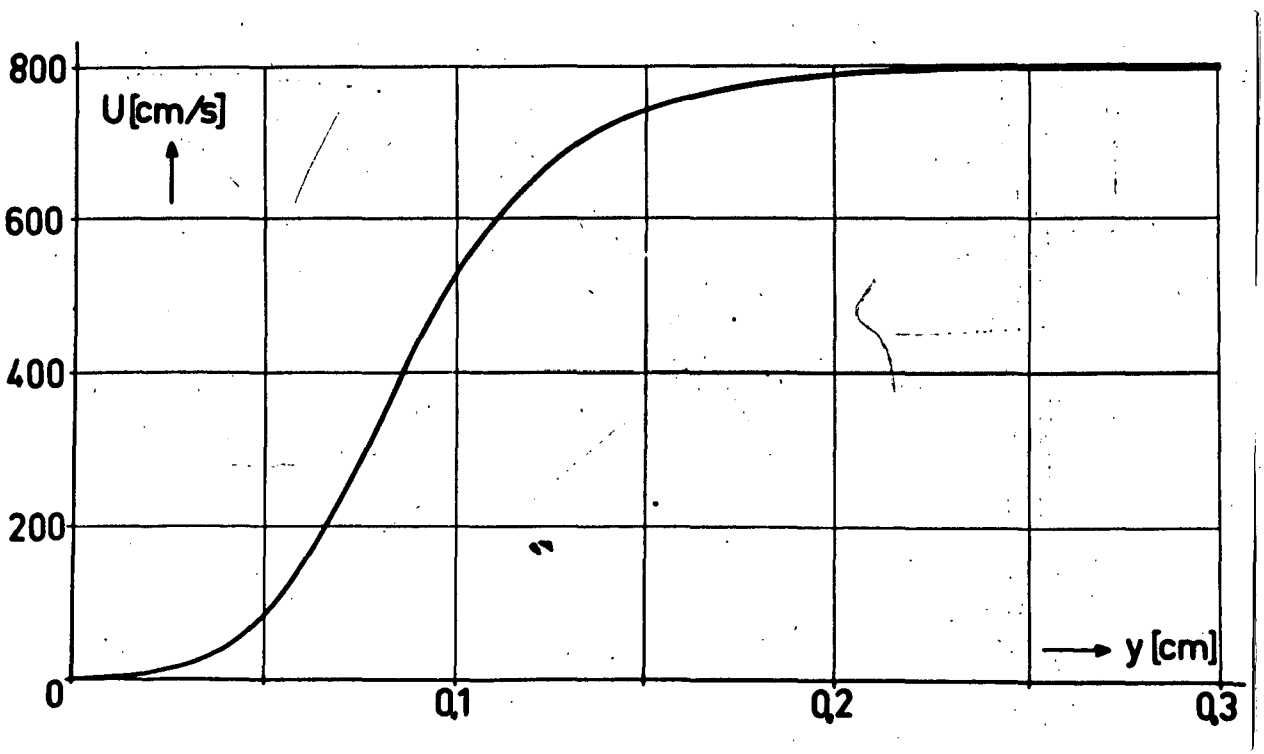

Figure 10a. Velocity profile U_0 = 800 cm/sec; D = 7.5 cm; x = 0 cm.

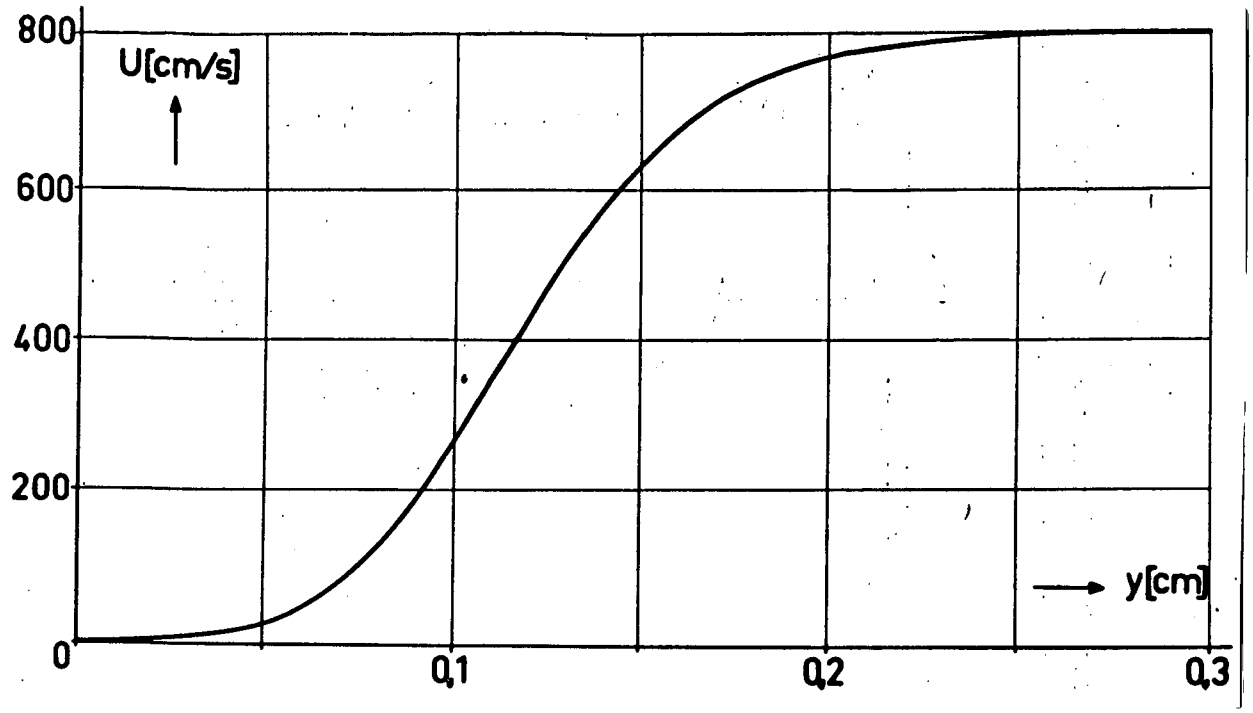

Figure 10b. Velocity profile U_o = 800 cm/sec; D = 7.5 cm; x = 0 cm.

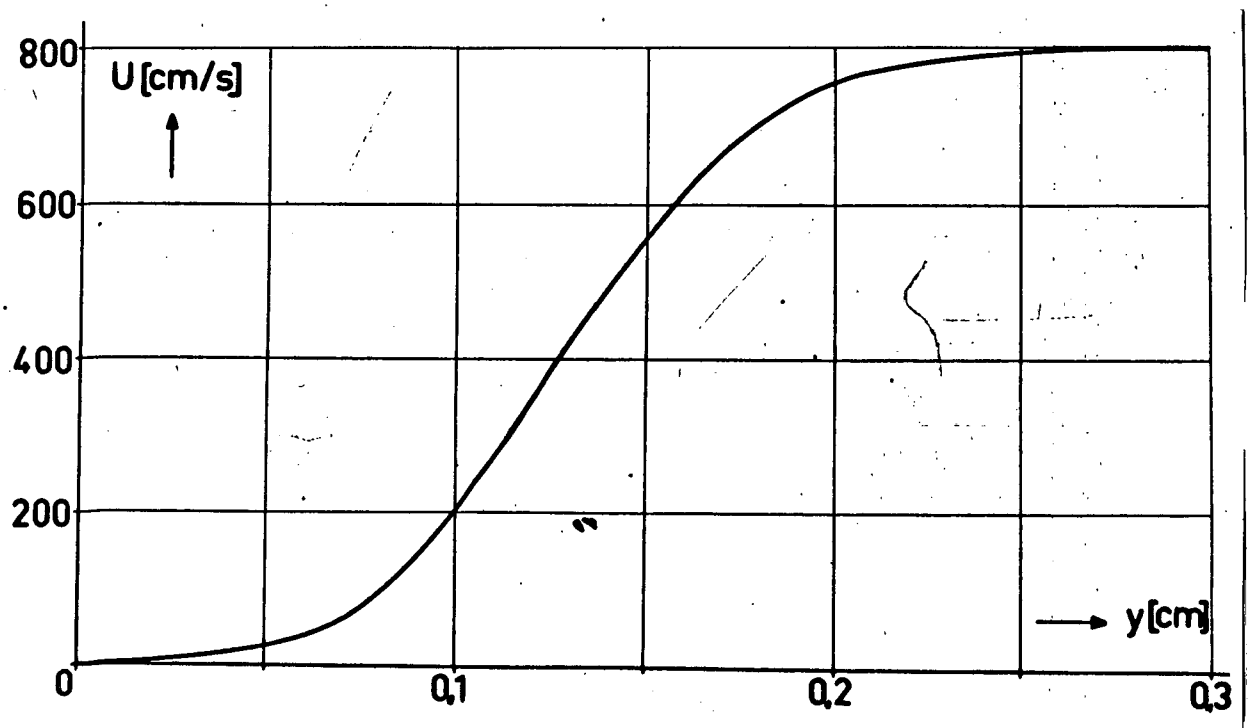

Figure 10c. Velocity profile U_o = 800 cm/sec; D = 7.5 cm; x = 0 cm.

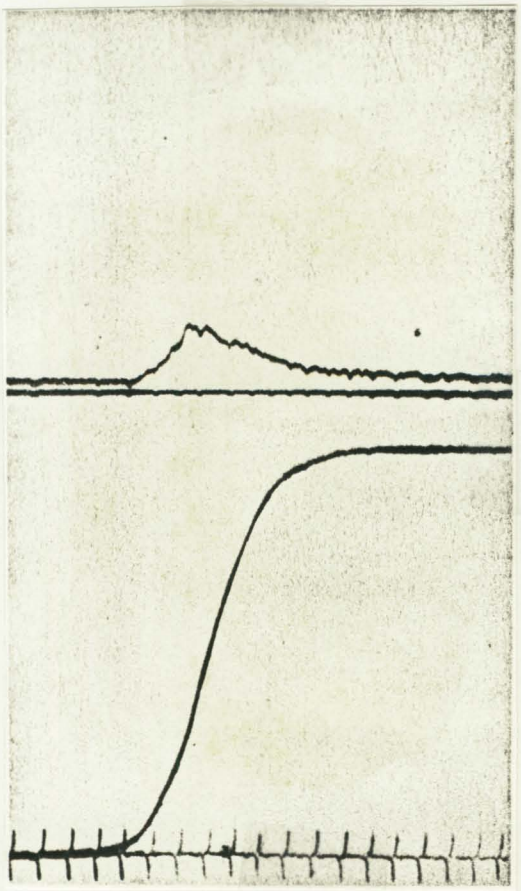

Figure 11a. Velocity and amplitude variation for U_o = 8 m/sec; f = 416 Hz; x = 0.04 cm.

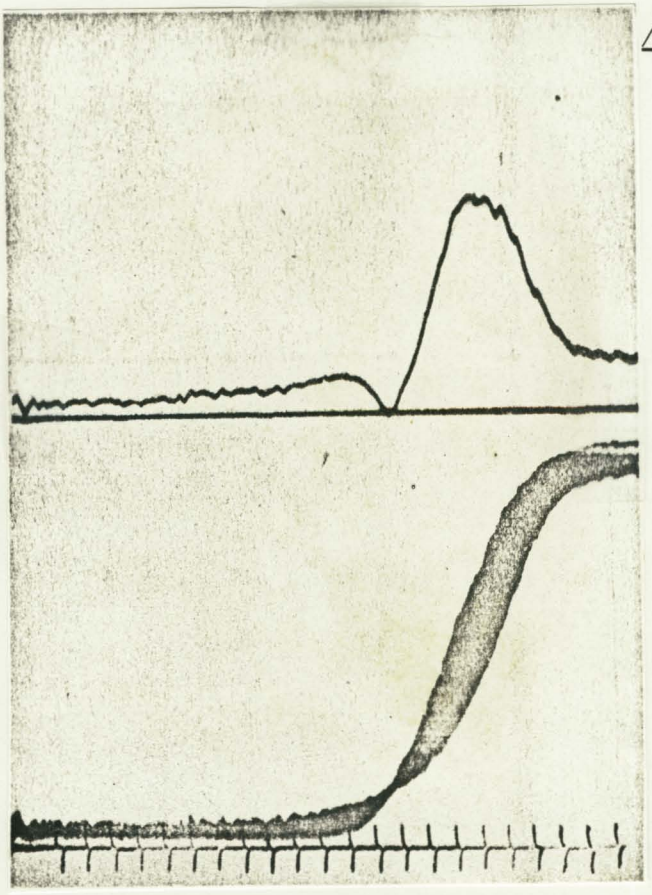

Figure 11b. Velocity and amplitude variation for U_o = 8 m/sec; f = 416 Hz; x = 1.5 cm.

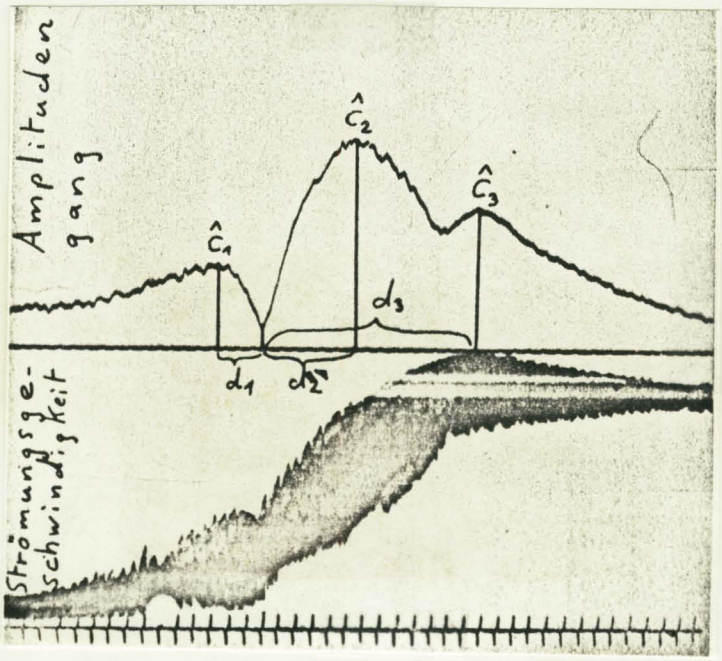

Figure 11 c. Velocity and amplitude variation for U_o = 8 m/sec; f = 416 Hz; x = 2.6 cm.

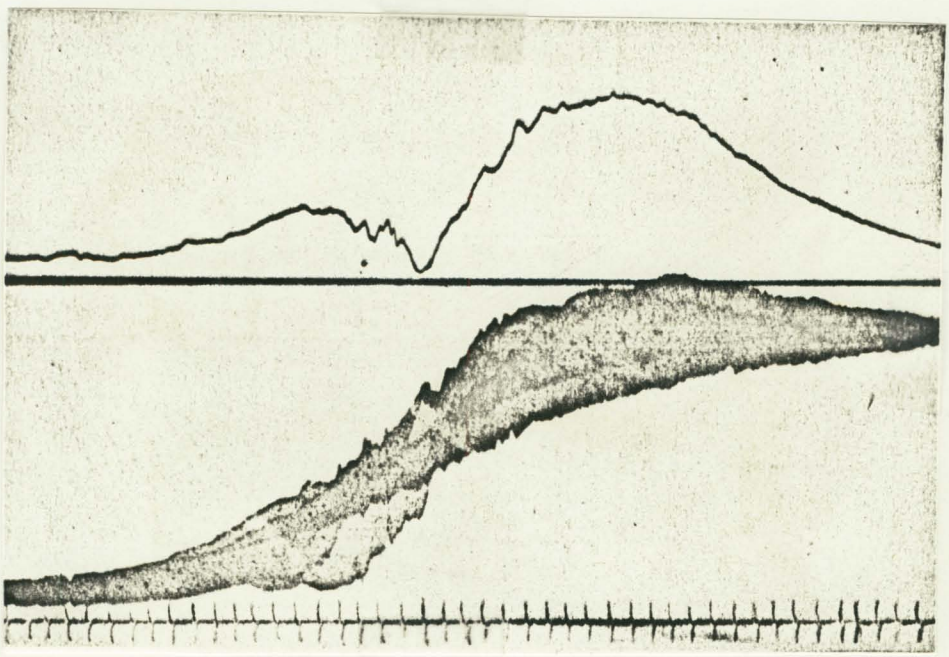

Figure 11d. Velocity and amplitude variation for U_o = 8 m/sec; f = 416 Hz; x = 3.2 cm.

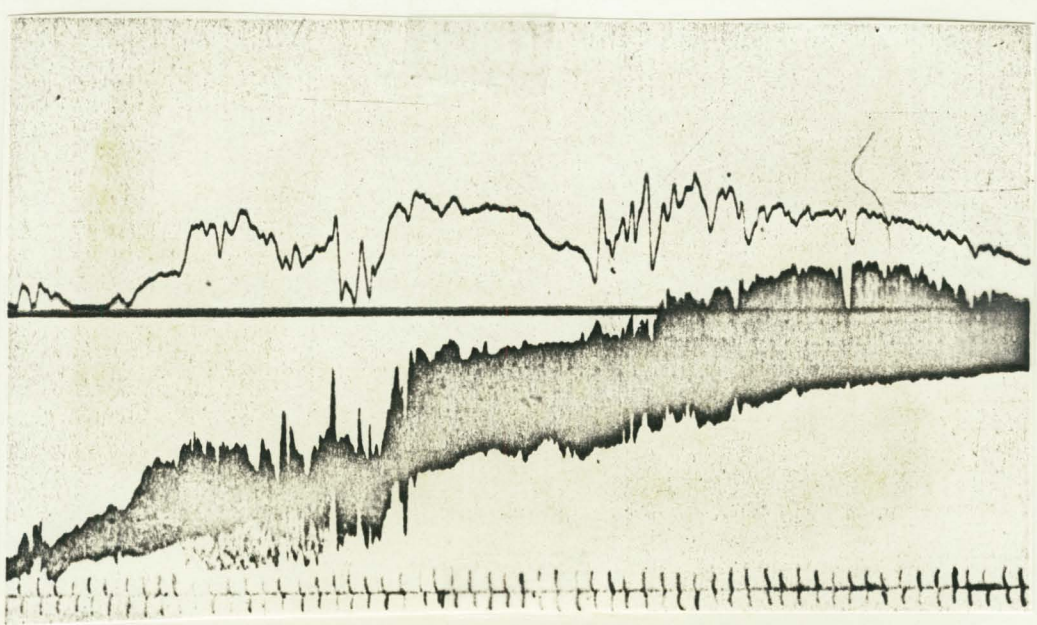

Figure 11e. Velocity and amplitude variation for U_o = 8 m/sec; f = 416 Hz; x = 4 cm.

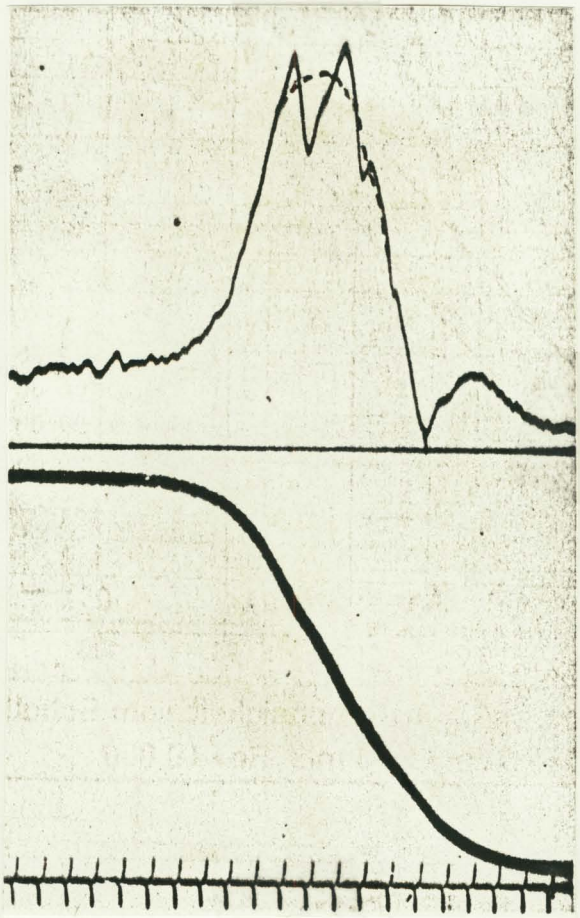

Figure 12. Peaking of the $\hat{c}_2$ maximum at low amplitude.

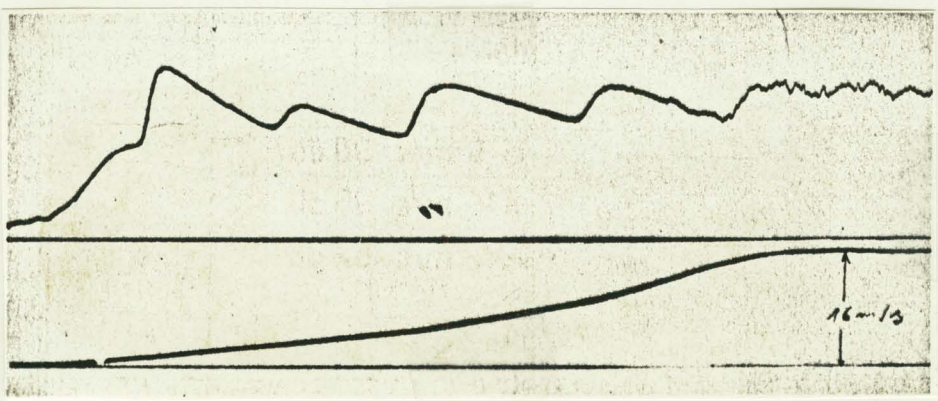

Figure 13. Analysis of the sound variation with flow velocity declining with time and constant sound pressure.

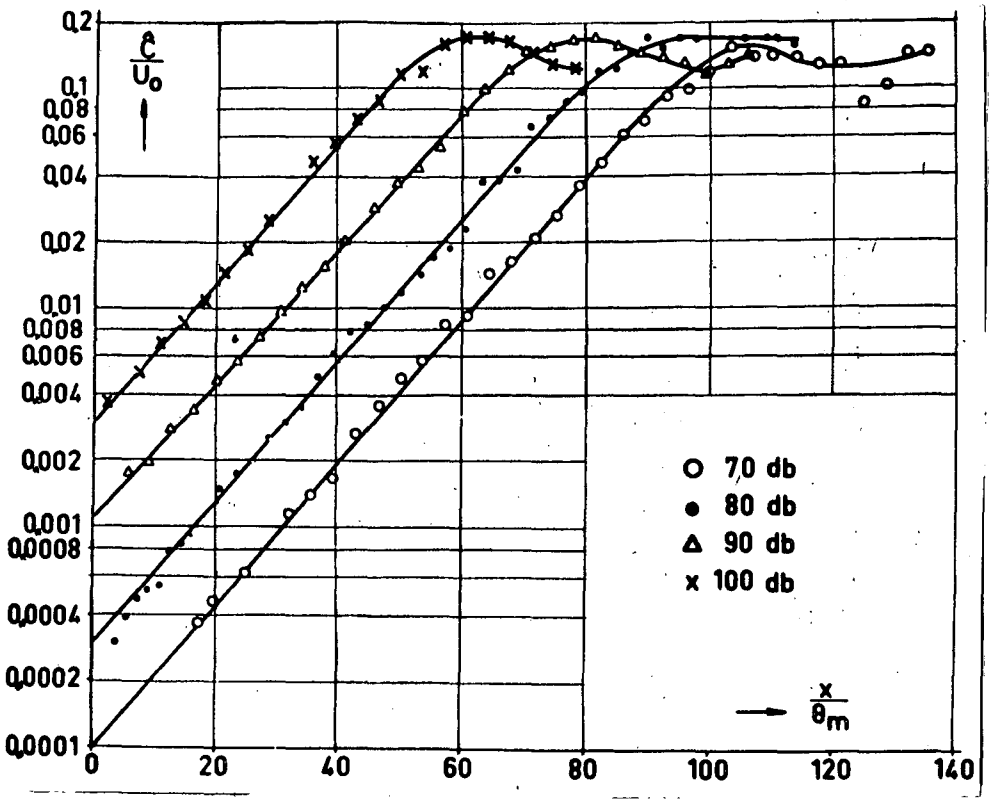

Figure 14. $\hat{C}_2/U_o$ excitation as a function of sound pressure D = 7.5 cm; U_o = 8 m/sec; Re = 40,000.

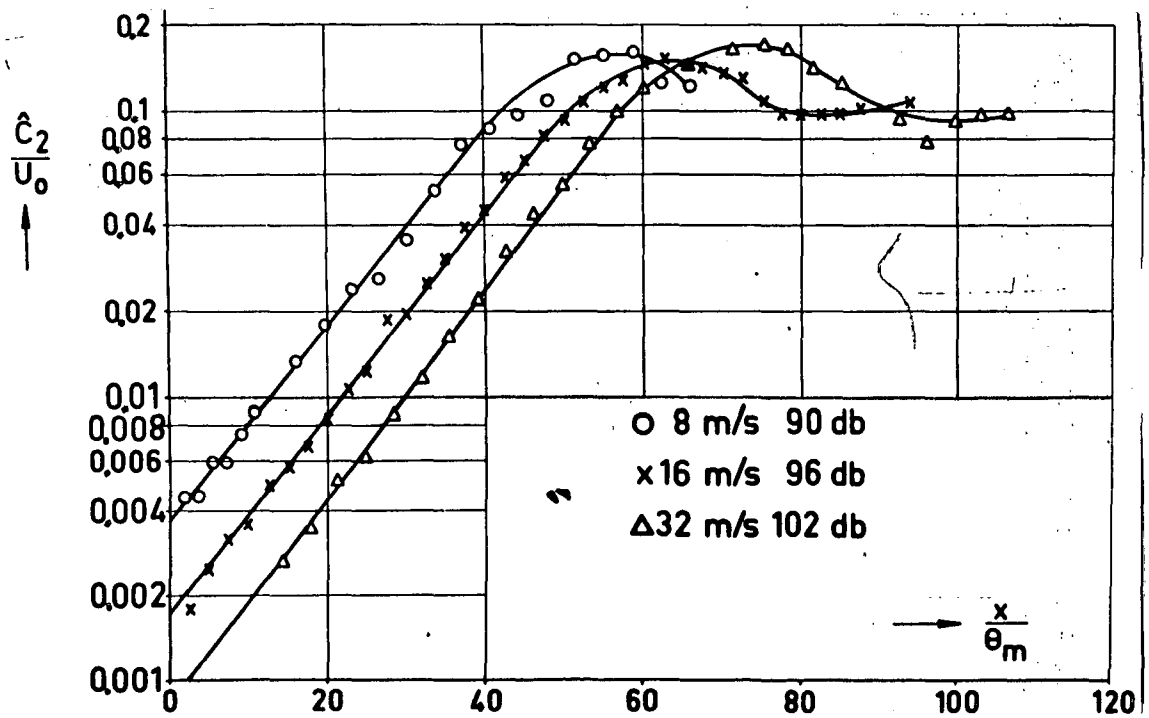

Figure 15. $\hat{C}_2/U_o$ excitation function of velocity and sound intensity D = 7.5 cm; S = 0.0118.

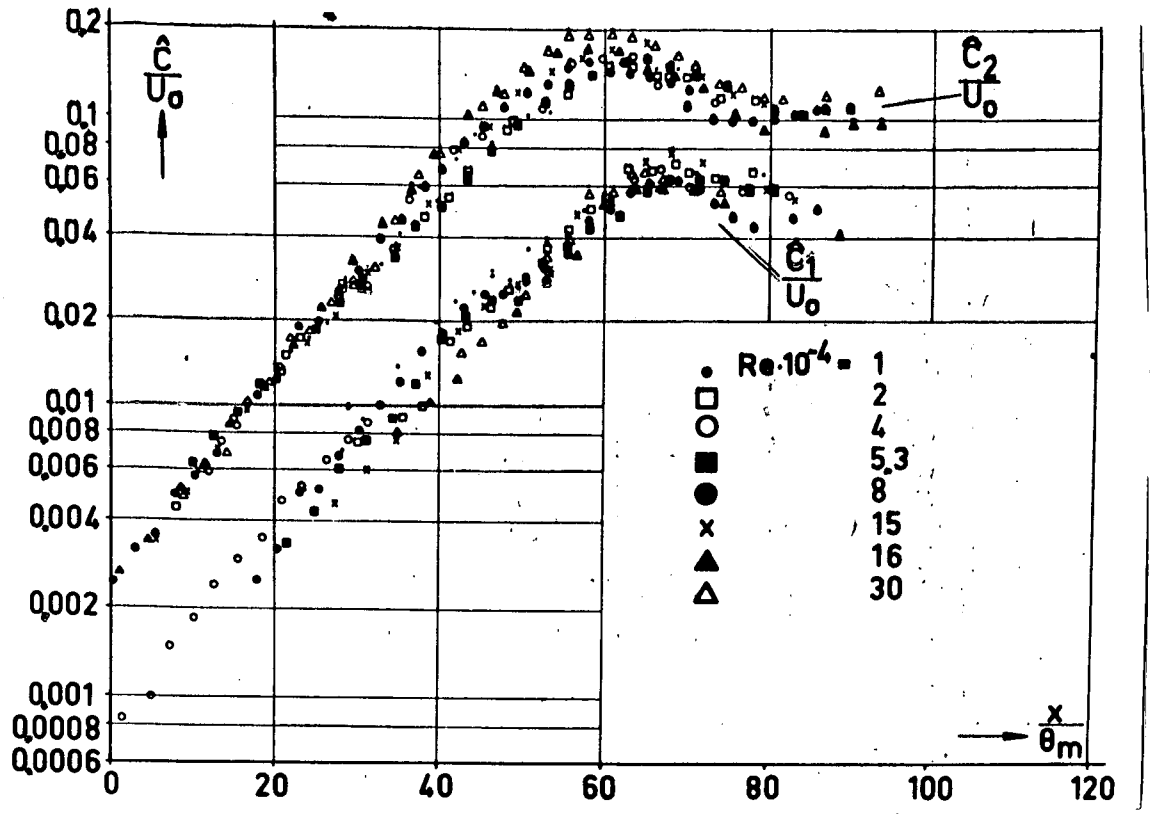

Figure 16. Excitation $\hat{C}_1/U_o$ and $\hat{C}_2/U_o$ for Re = 10^4-$3\cdot10^5$, S=0.0118

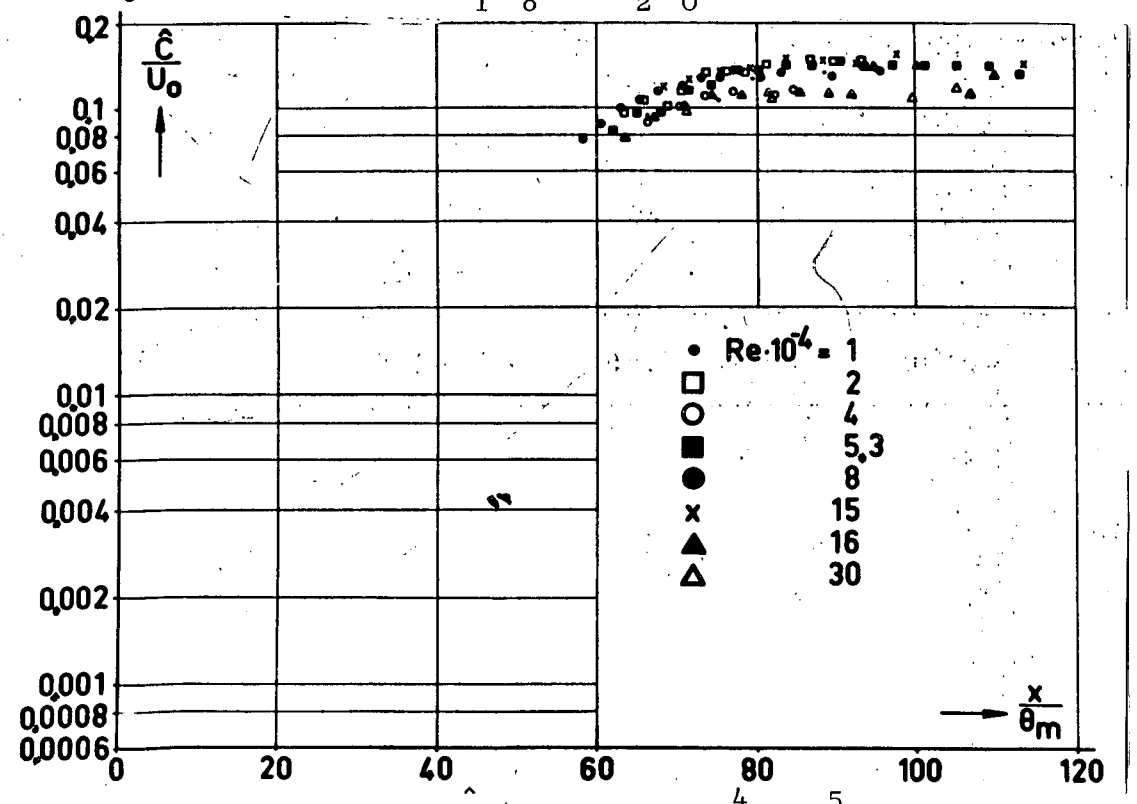

Figure 17. Excitation $\hat{C}_3/U_o$ for Re = 10^4-$3\cdot10^5$, S = 0.0118.

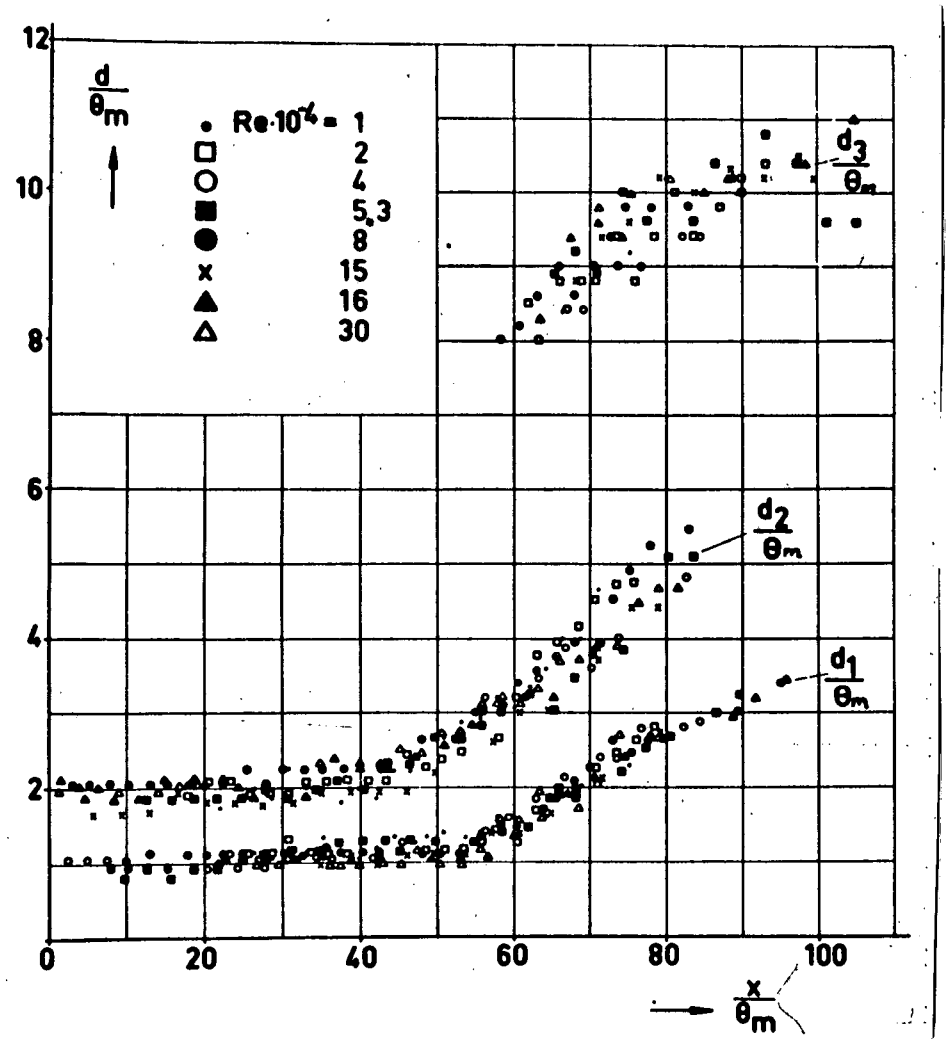

Figure 18. Distance curves for Re = 10^4-$3 \cdot 10^5$, S = 0.0118.

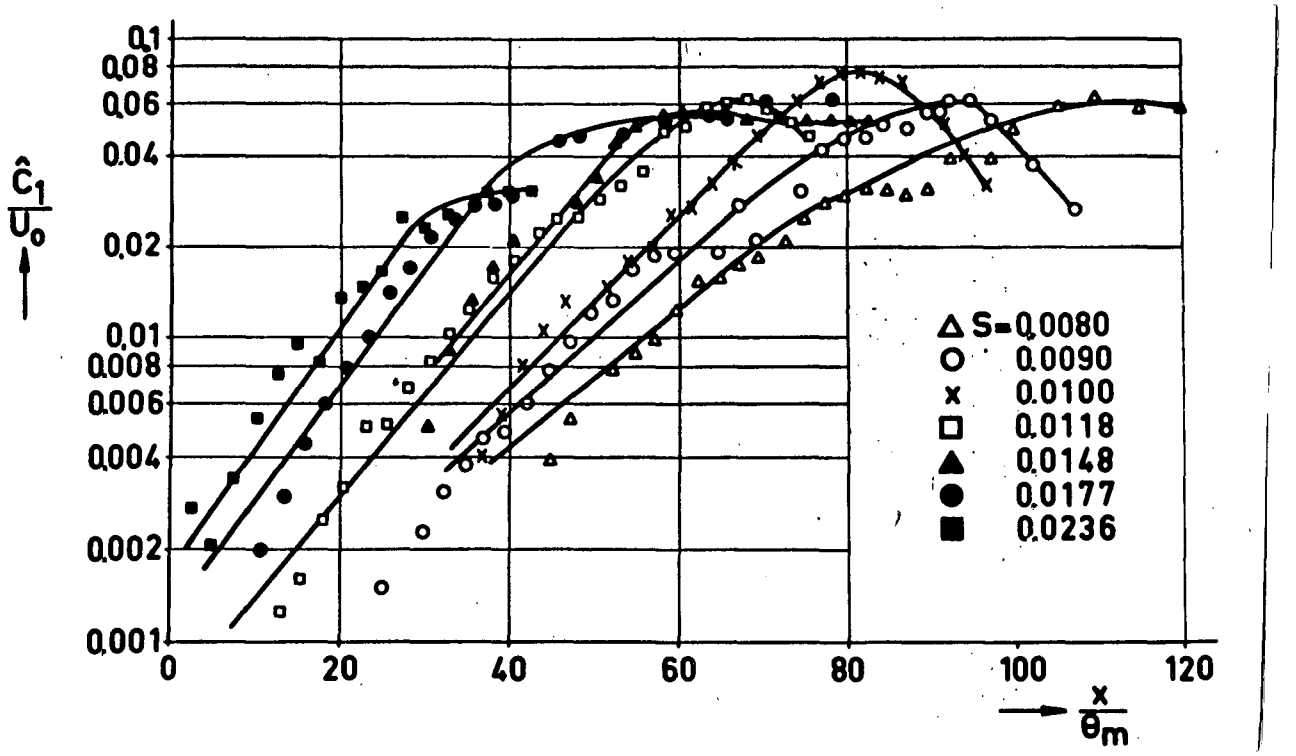

Figure 19. Excitation $\hat{C}_1/U_o$ for various Strouhal numbers, D = 75 cm, U_o = 16 m/sec, Re_D = 80,000.

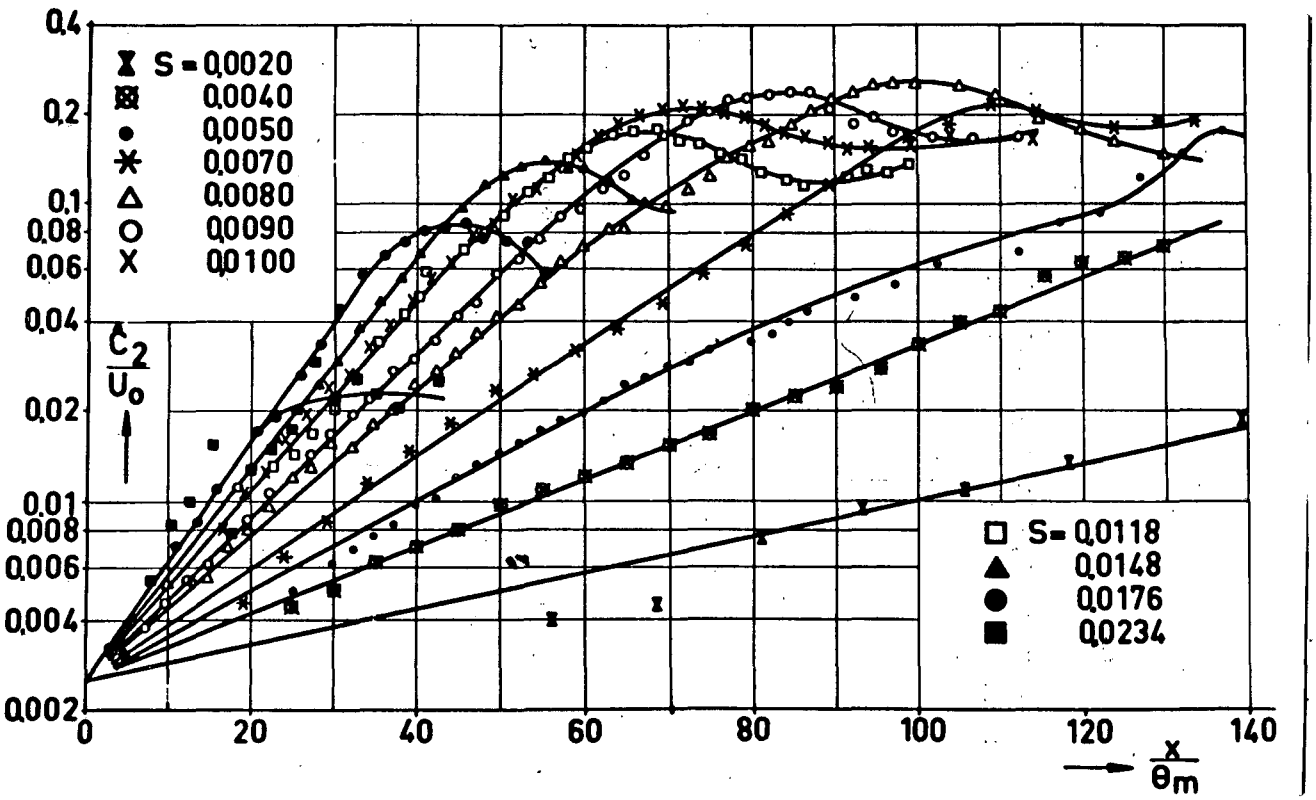

Figure 20. Excitation $\hat{C}_2/U_O$ for various Strouhal numbers, $D = 7.5$ cm, $U_O = 16$ m/sec, $Re_D = 80{,}000$.

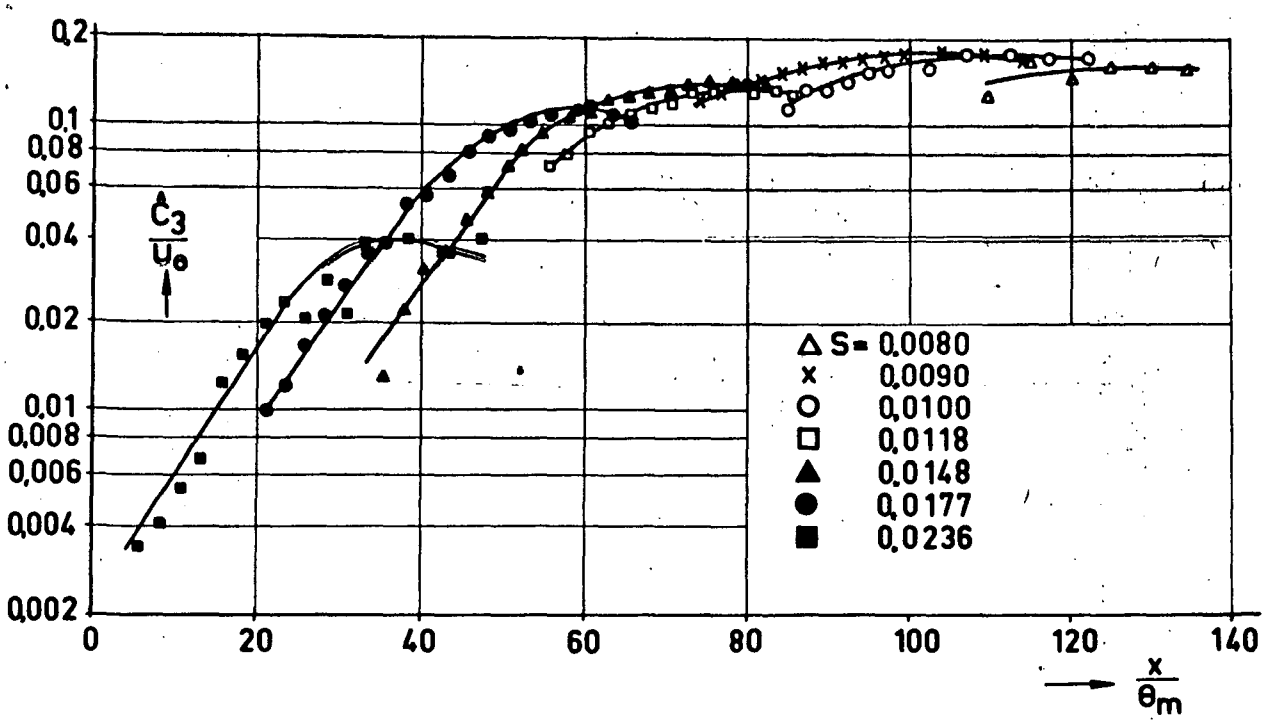

Figure 21. Excitation $\hat{C}_3/U_0$ for various strouhal numbers, D = 7.5 cm, U_0 = 16 m/sec, Re_D = 80,000.

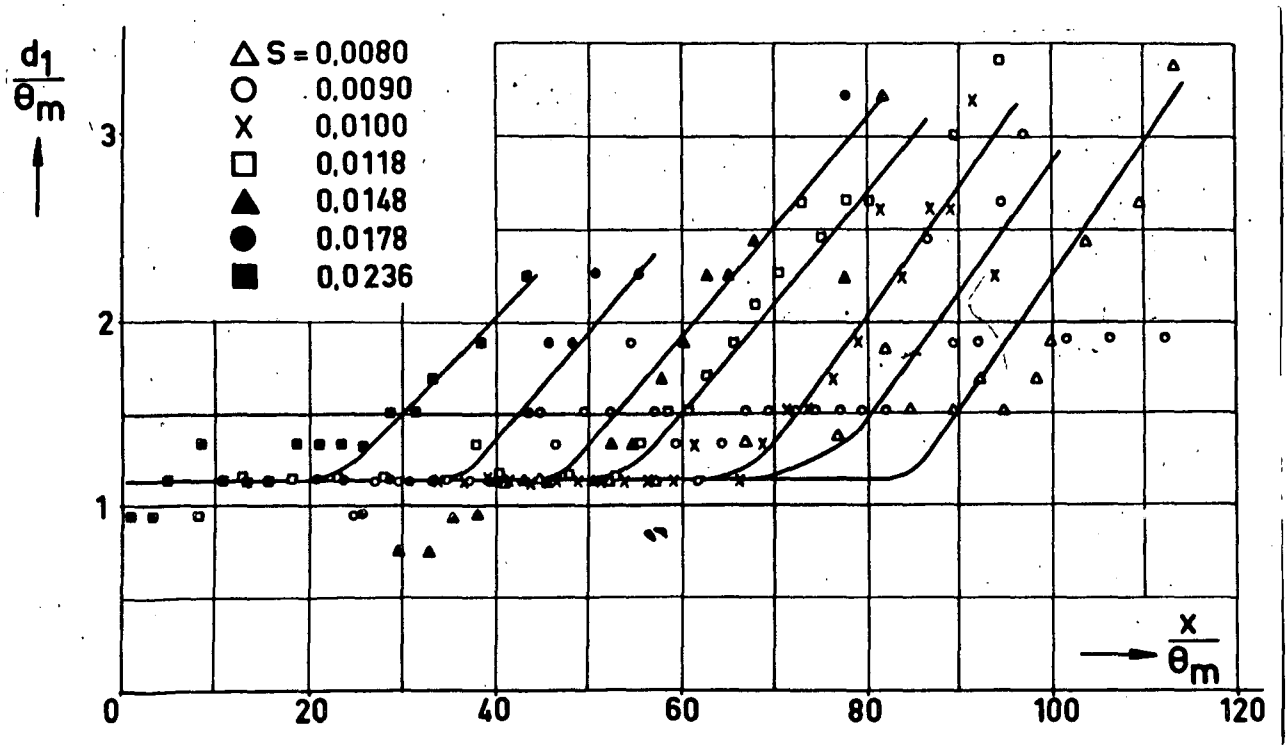

Figure 22. d_1/θ_m distance at various Strouhal numbers, D = 7.5 cm, U_0 = 16 m/sec, Re_D = 80,000.

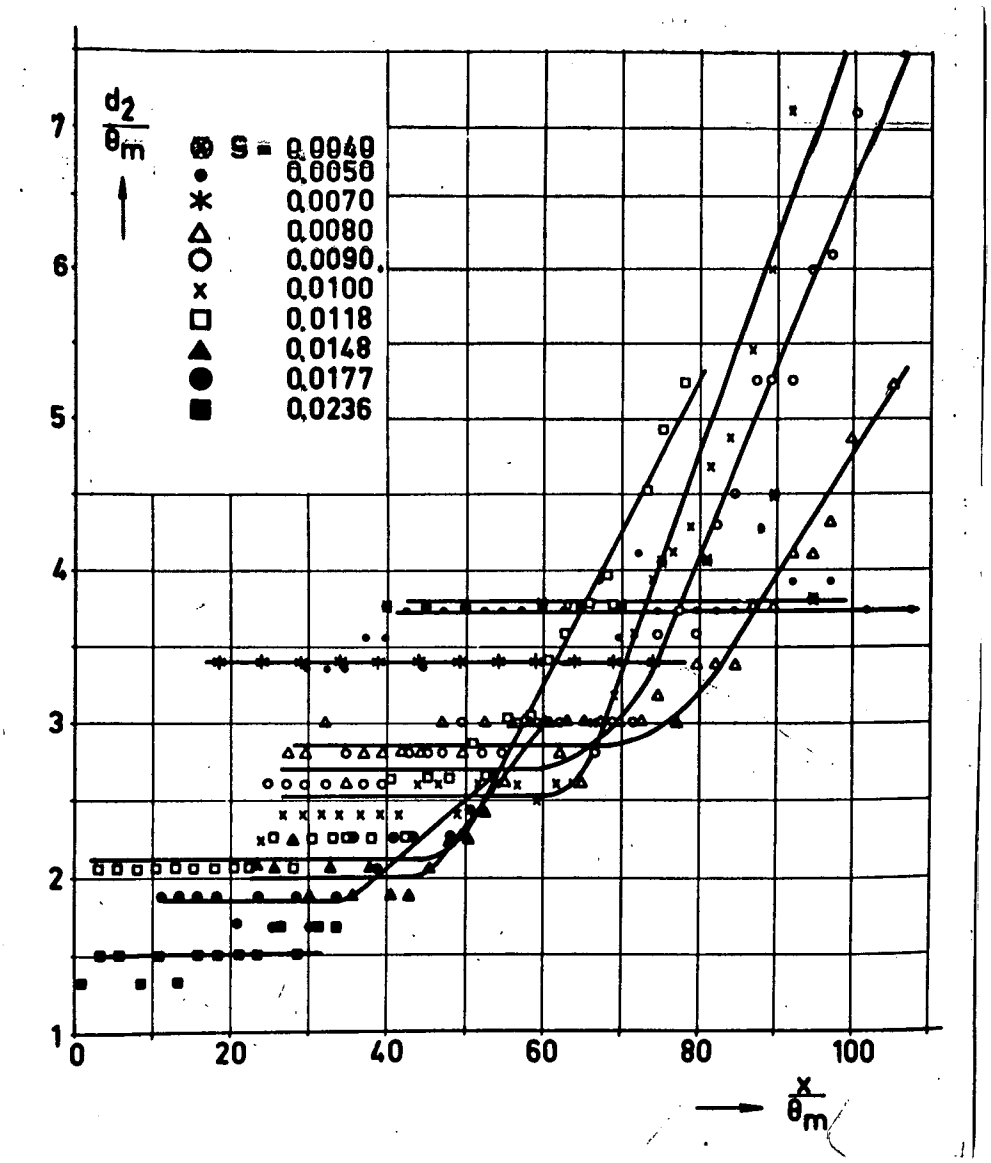

Figure 23. d_2/θ_m distance at various Strouhal numbers, D = 7.5 cm, U_o = 16 m/sec, Re_D = 80,000.

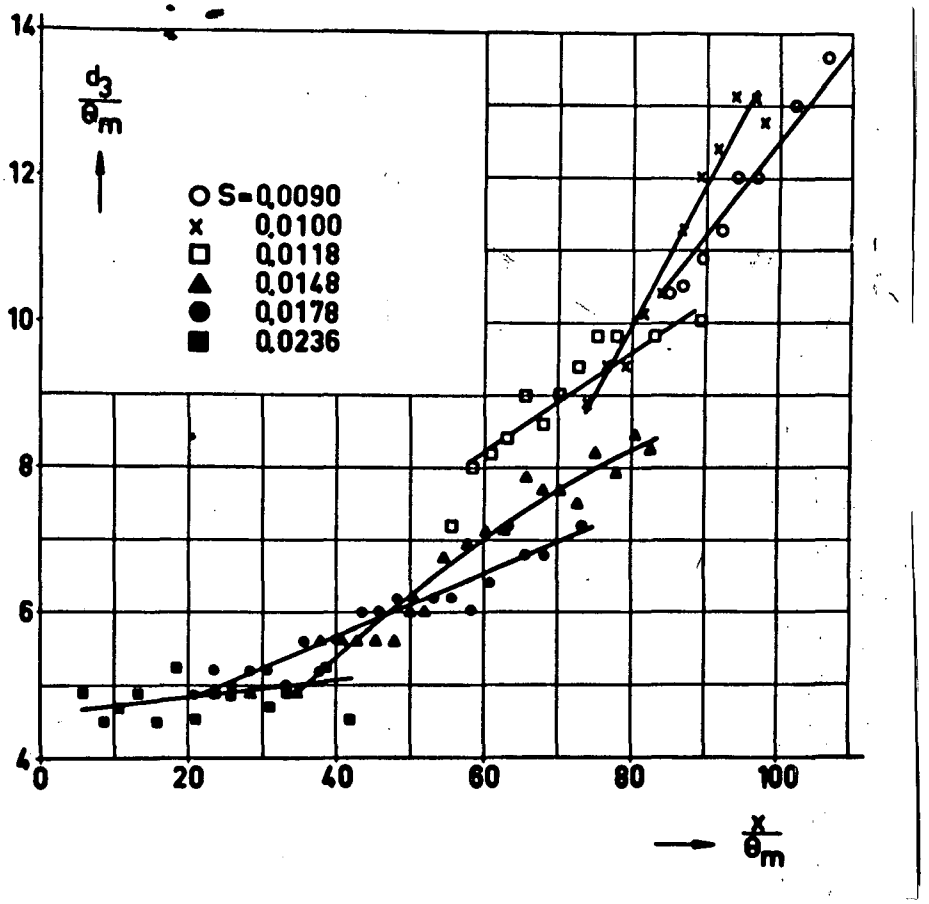

Figure 24. d_3/θ_m distance for various Strouhal numbers, D = 7.5 cm, U_o = 16 m/sec, Re = 80,000.

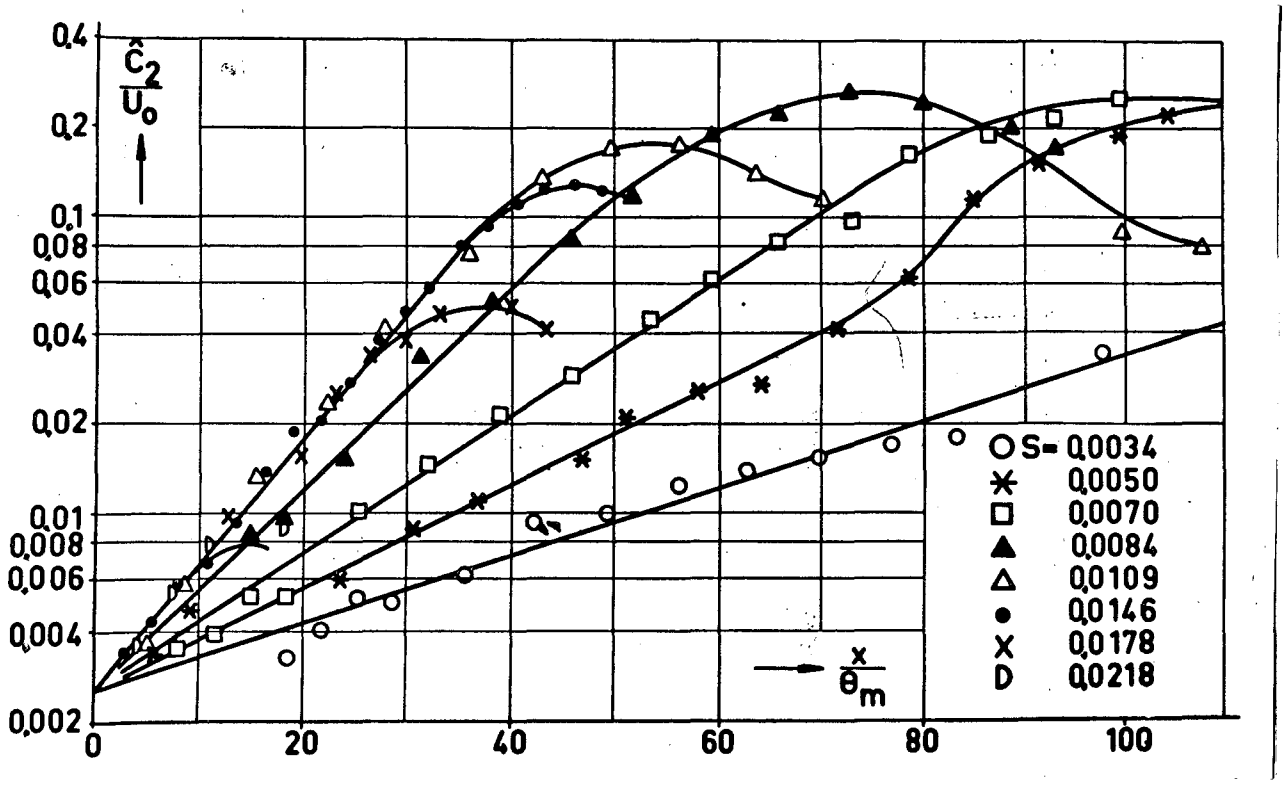

Figure 25. $\hat{C}_2/U_0$ excitation for various Strouhal numbers.
Flat nozzle U_0 = 8 m/sec, Re_h = 21,400.

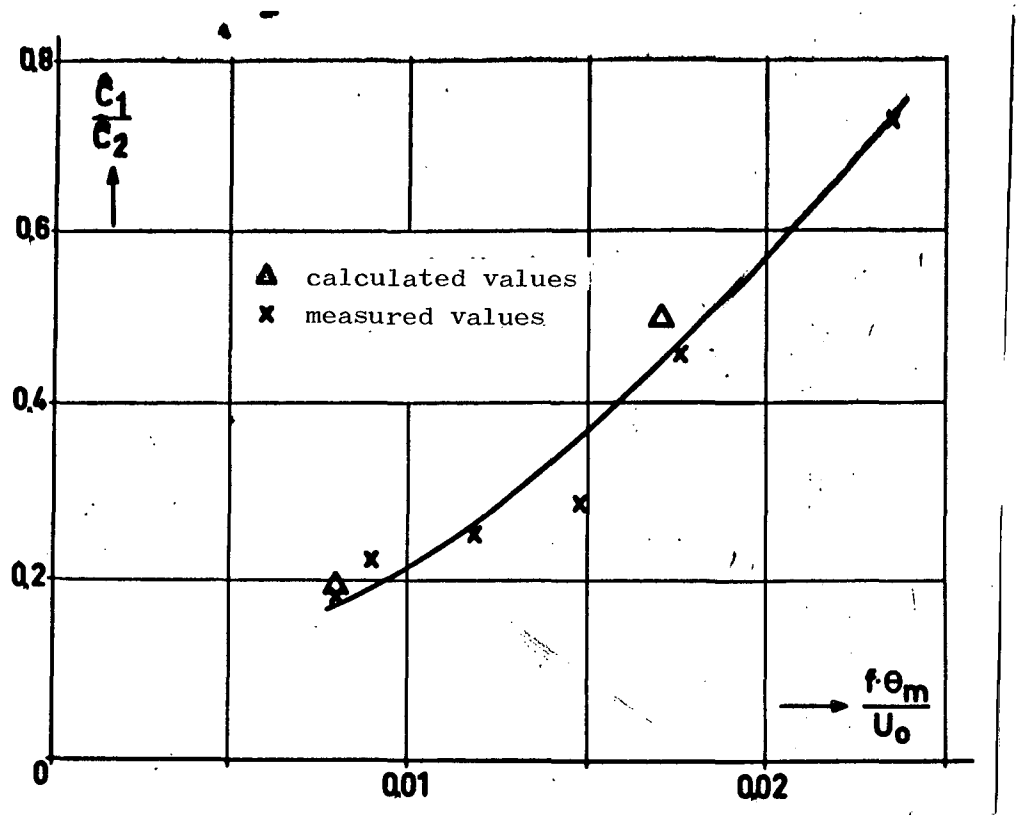

Figure 26. $\hat{C}_1/\hat{C}_2$ as a function of the Strouhal number.

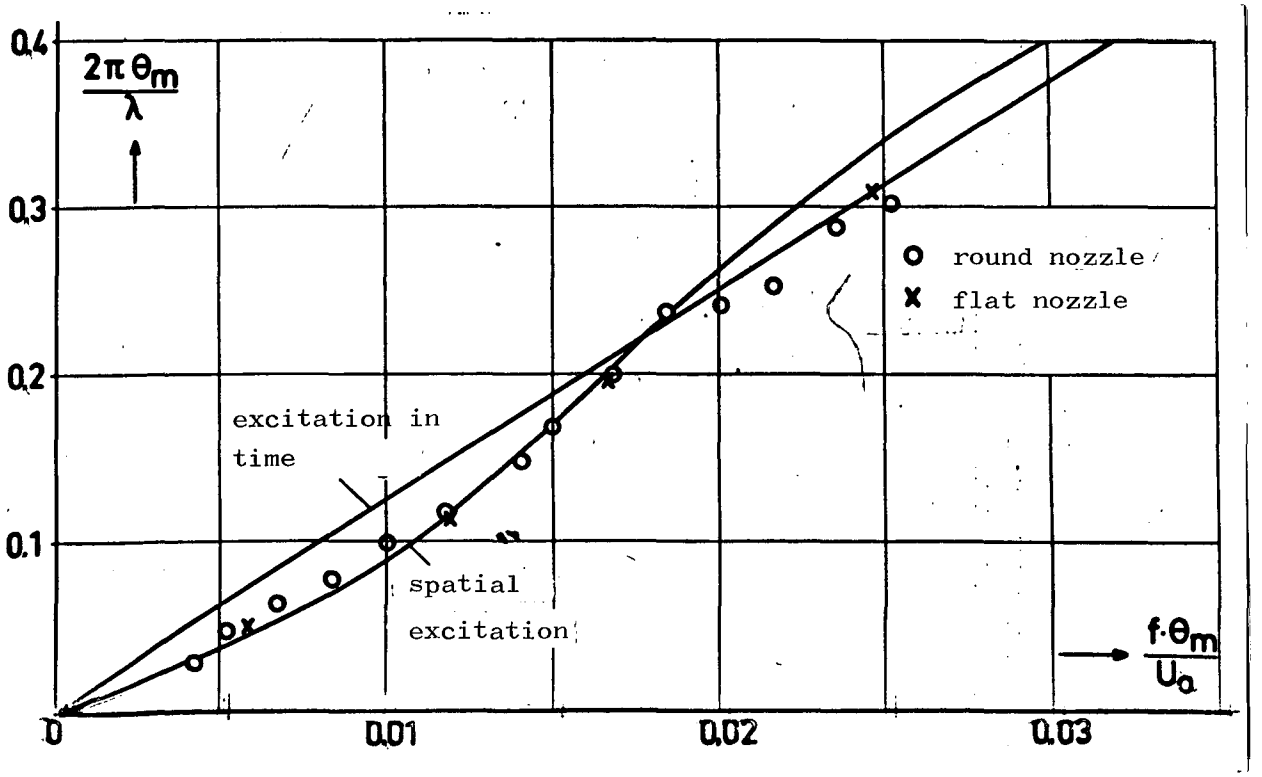

Figure 27. Theoretical and measured wave number as a function of the Strouhal number.

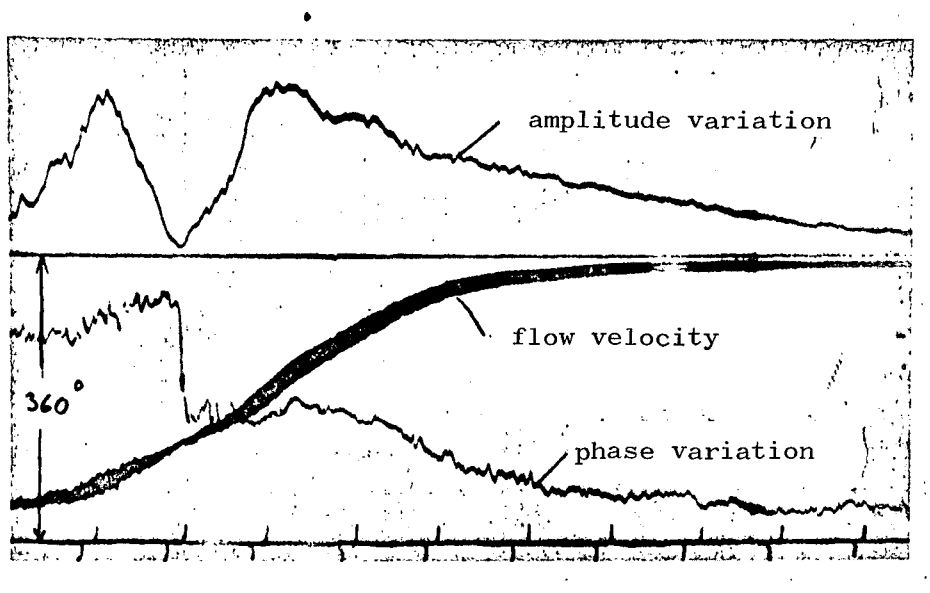

Figure 28. Phase variation, D = 7.5 cm; U_o = 16 m/sec; S = 0.018.

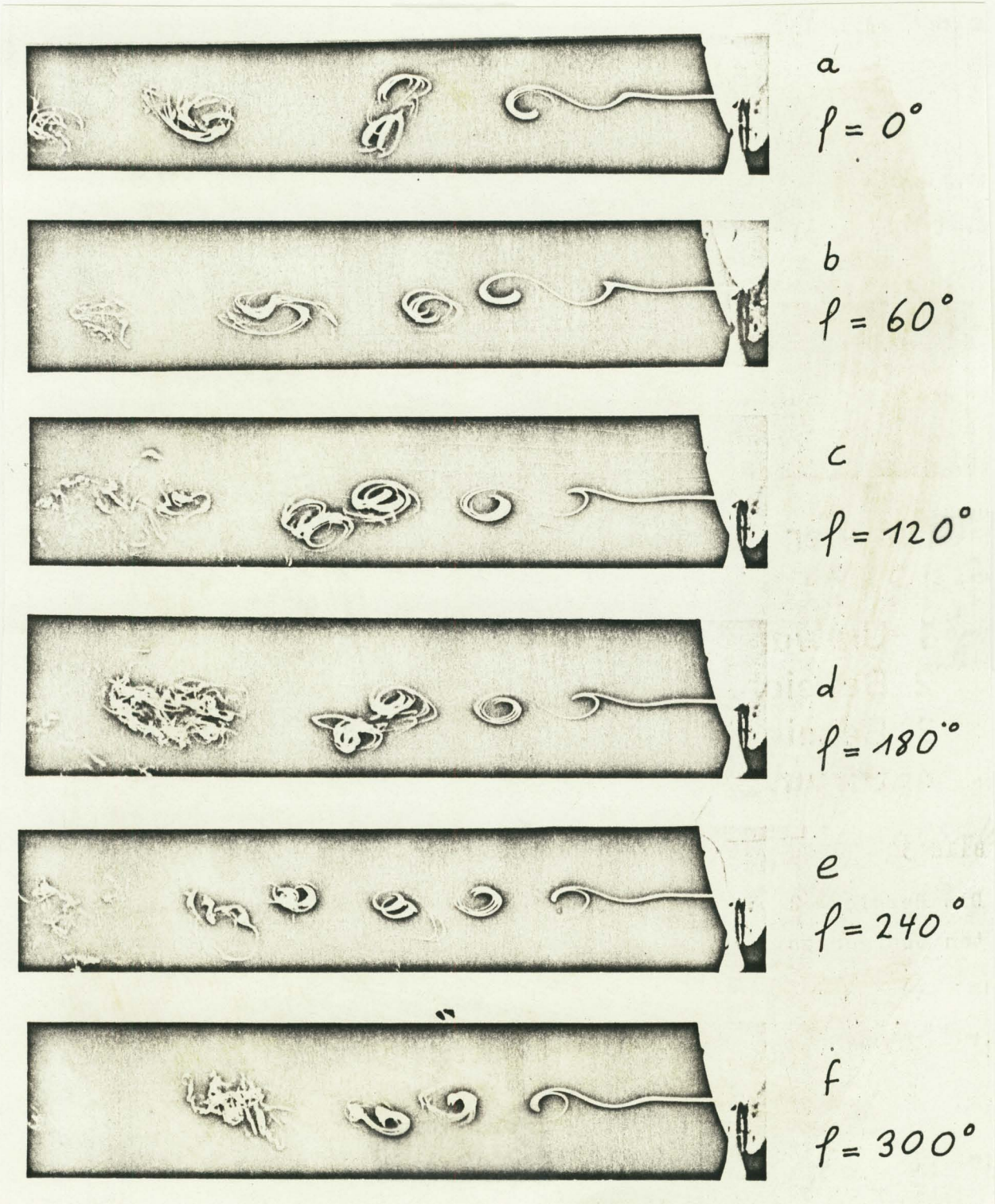

Figure 29. Progress of vortex roll-up, U_0 = 3 m/sec; f = 95 Hz.

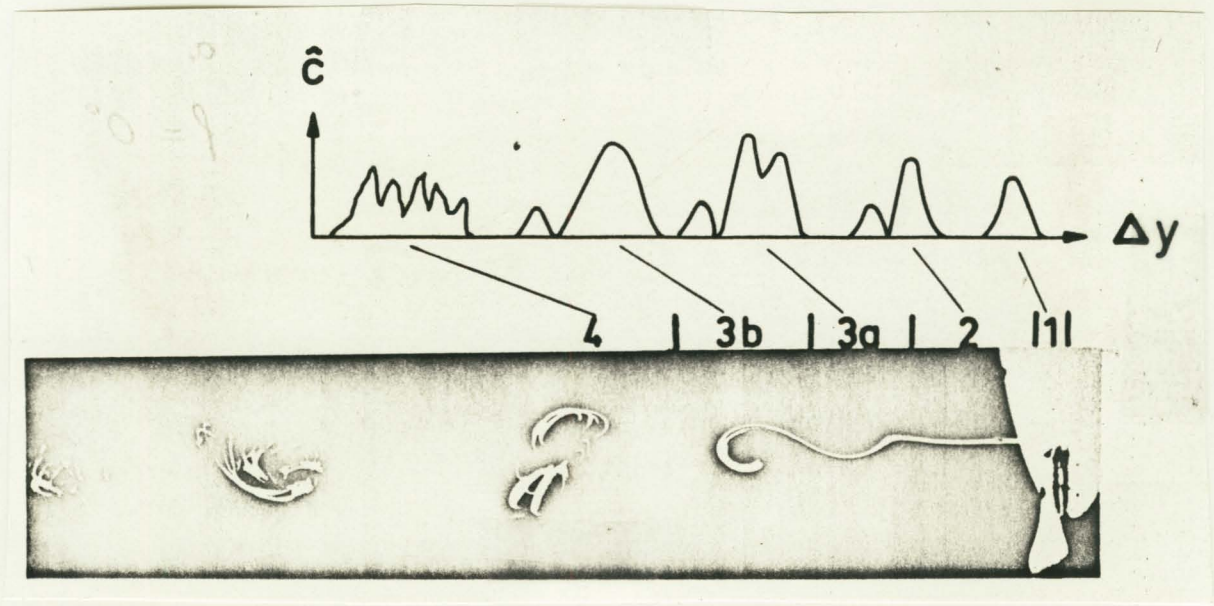

The four ranges of excitation.

1 - transformation range

2 - linear excitation range

3 - nonlinear excitation range

4 - turbulent range

Figure 30. Range 2 and 3 together form the range of laminar-turbulent transition. Turbulence begins in range 4.

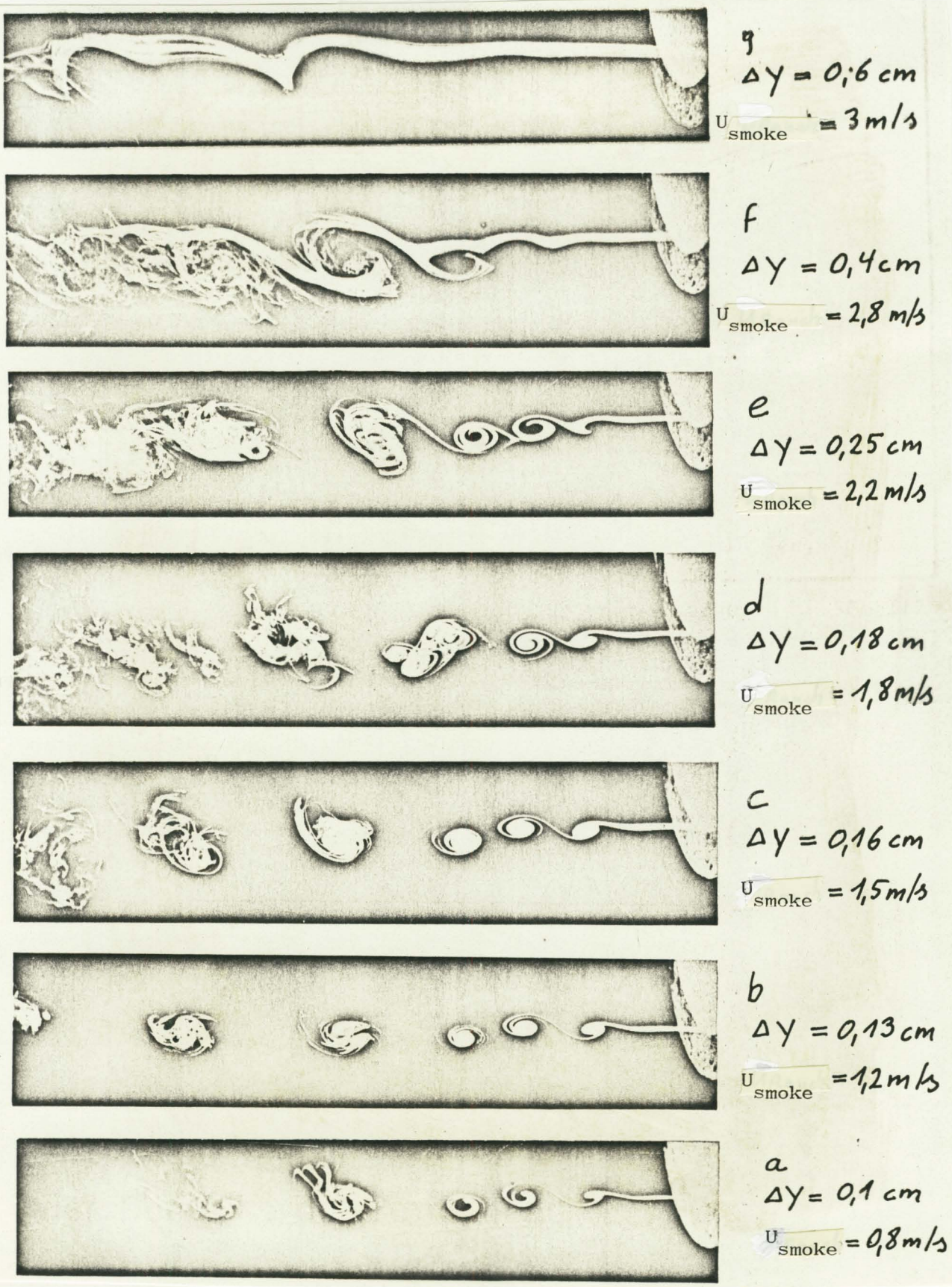

Figure 31. Vortex patterns with smoke injection at different Δy heights of the boundary layer. U_0=3 m/sec; f=95 Hz; D=7.5 cm.

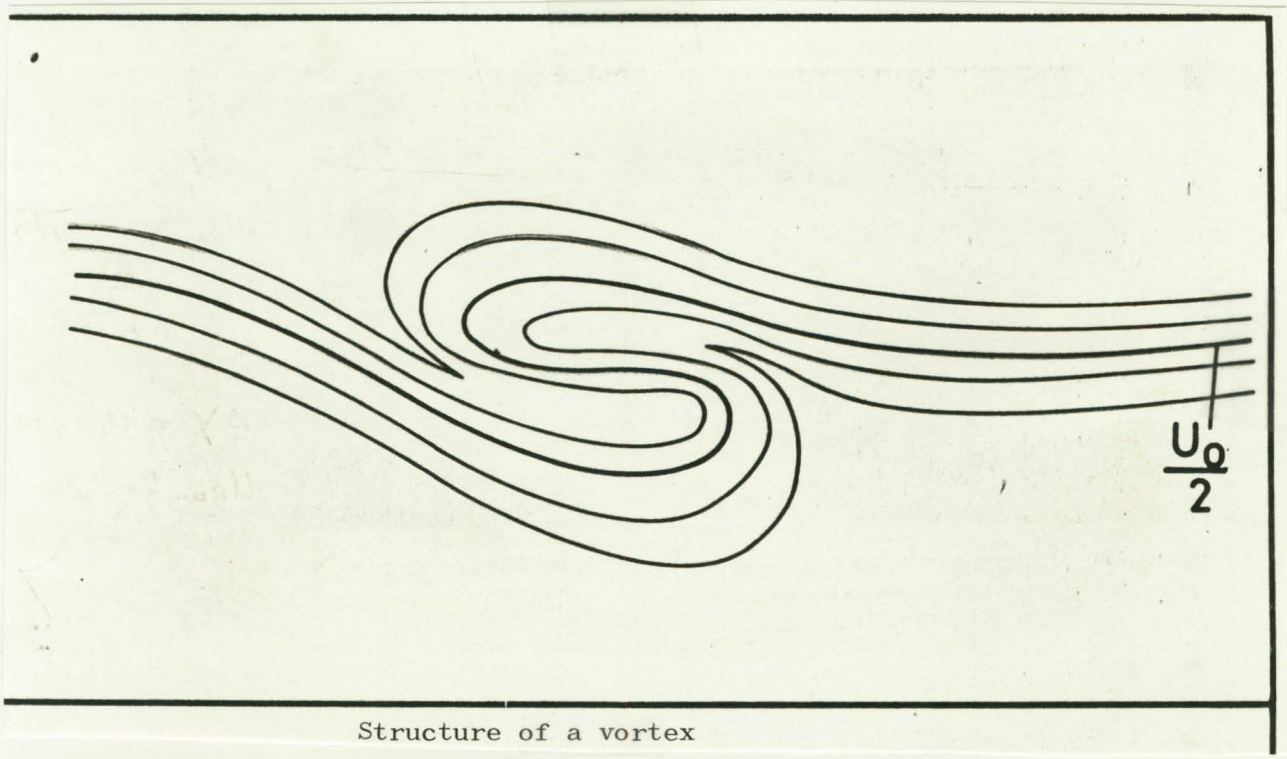

Figure 32. Structure of the first vortex from the right in Figure 31.

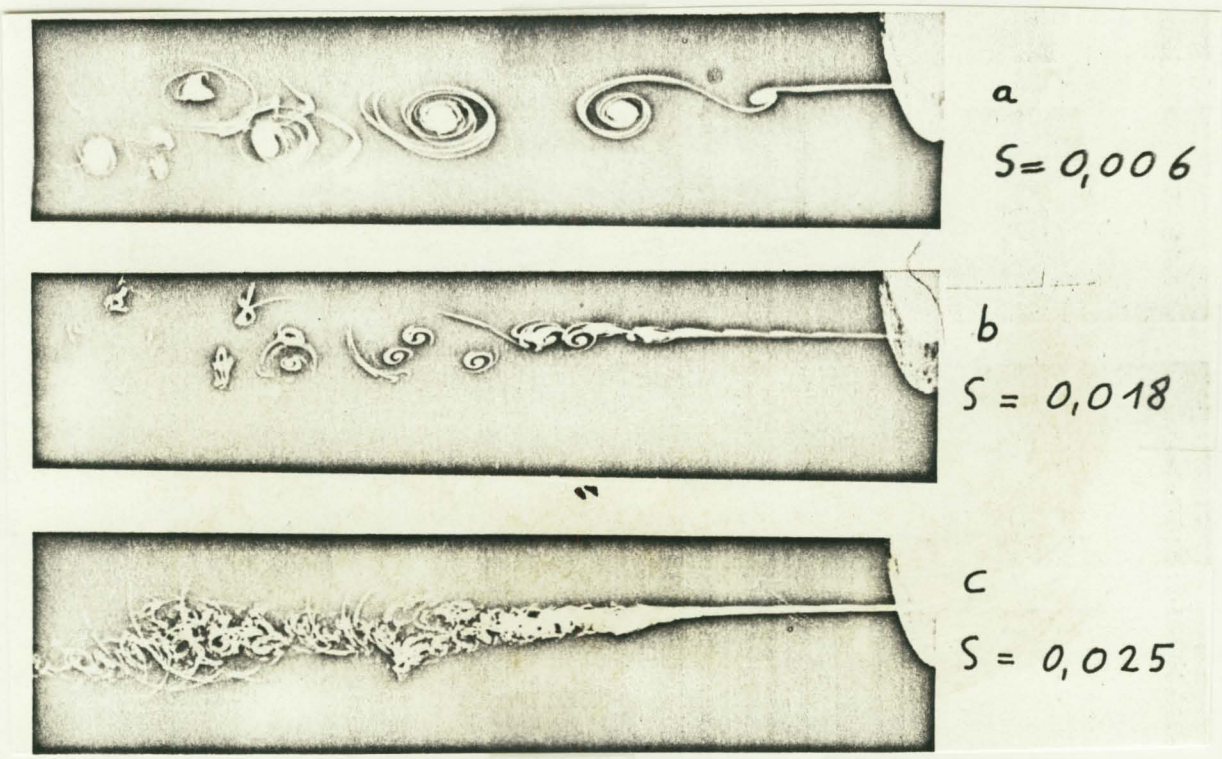

Figure 33. Dependence of a vortex pattern from the Strouhal number. U_0 = 3 m/sec.

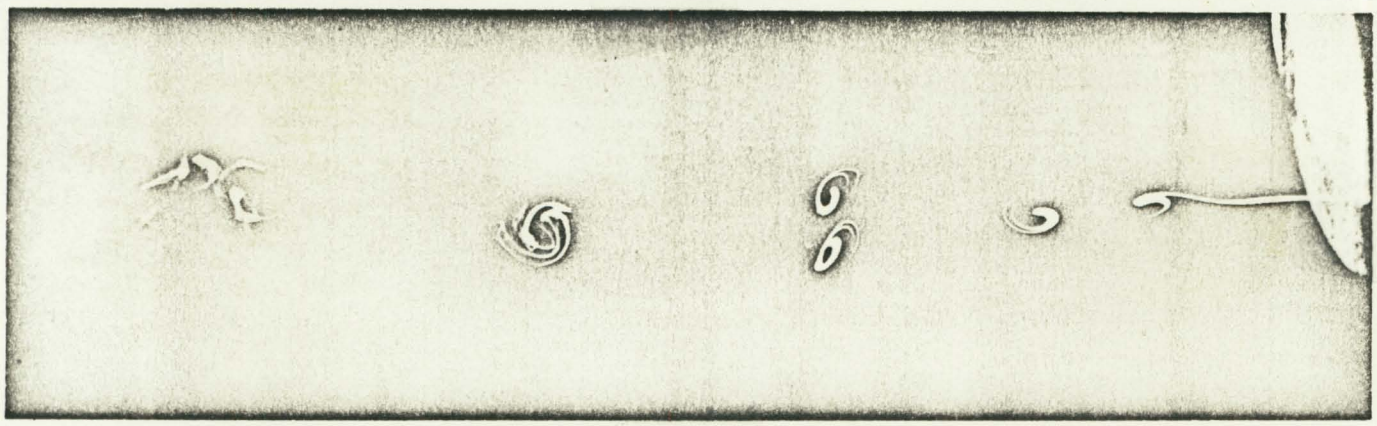

Figure 34. Stages of vortex development: roll-up, slippage, decomposition.

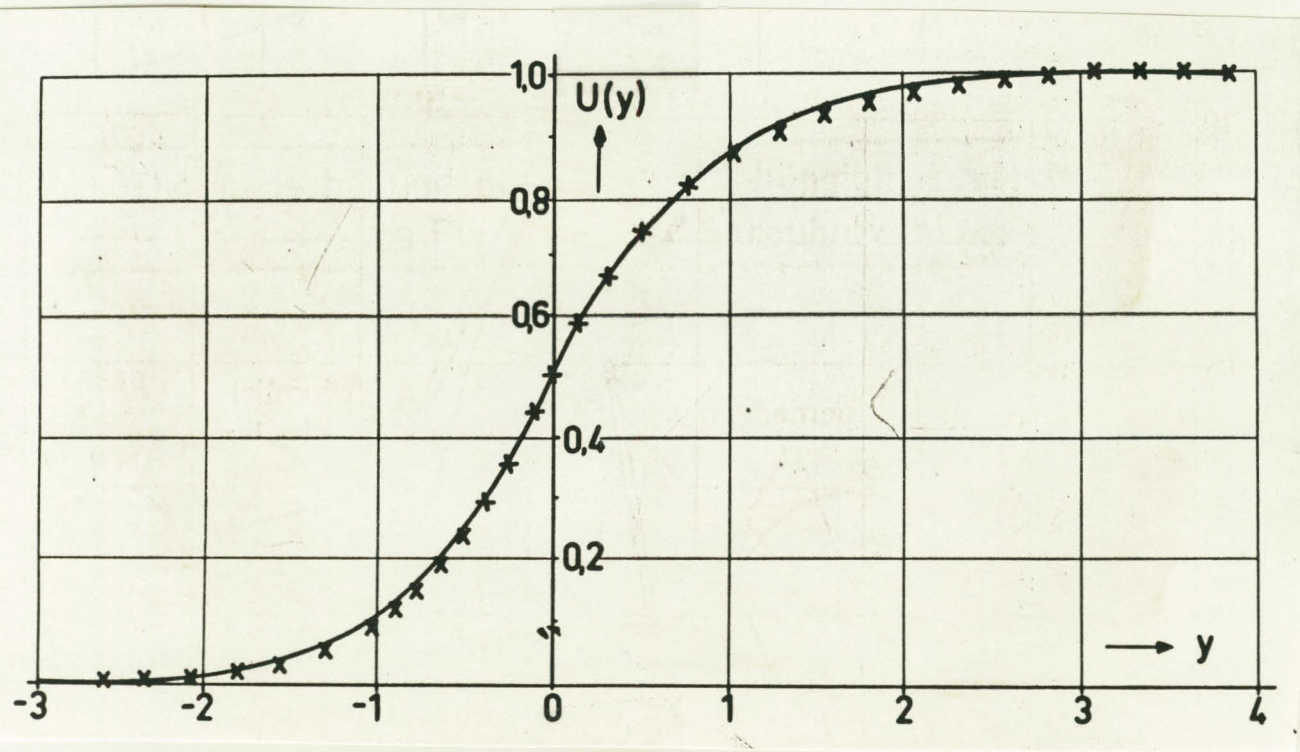

Figure 35. Tanh profile and measured velocity profile at $x/\theta_m = 10$; $U_o = 8$ m/sec; D = 7.5 cm, in dimensionless plotting.

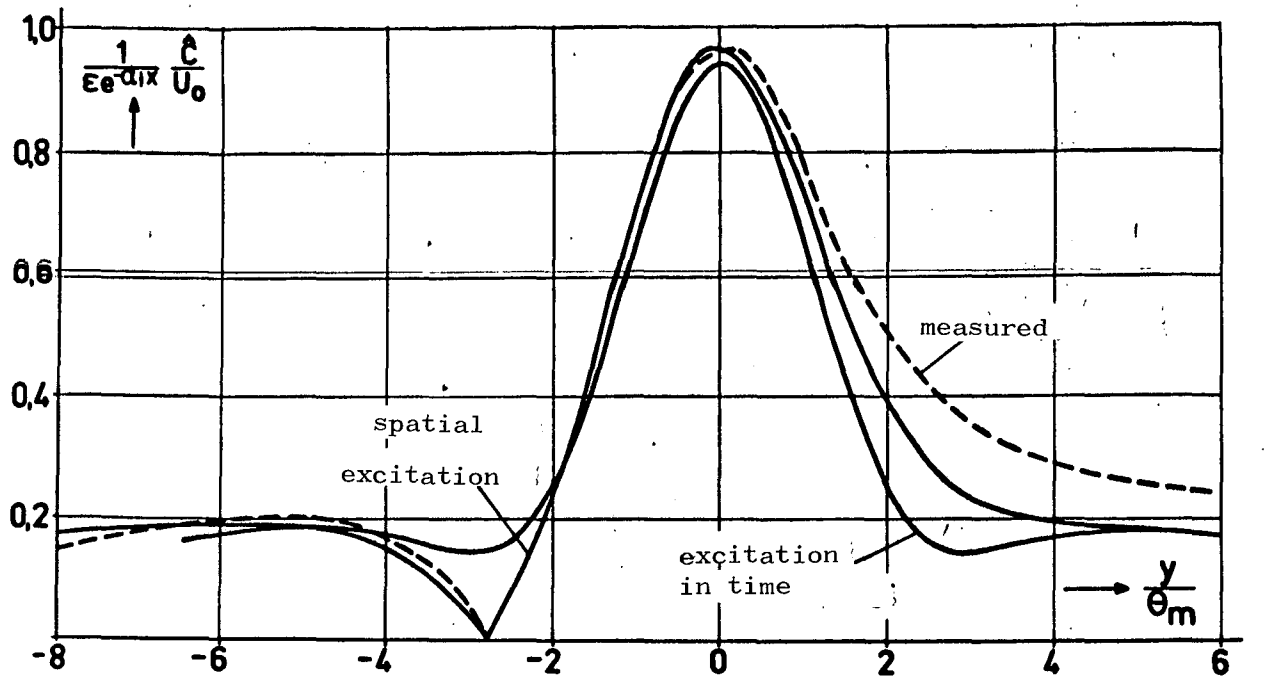

Figure 36. Theoretical and measured amplitude variation at $f \cdot \theta_m / U_o = 0.008$.

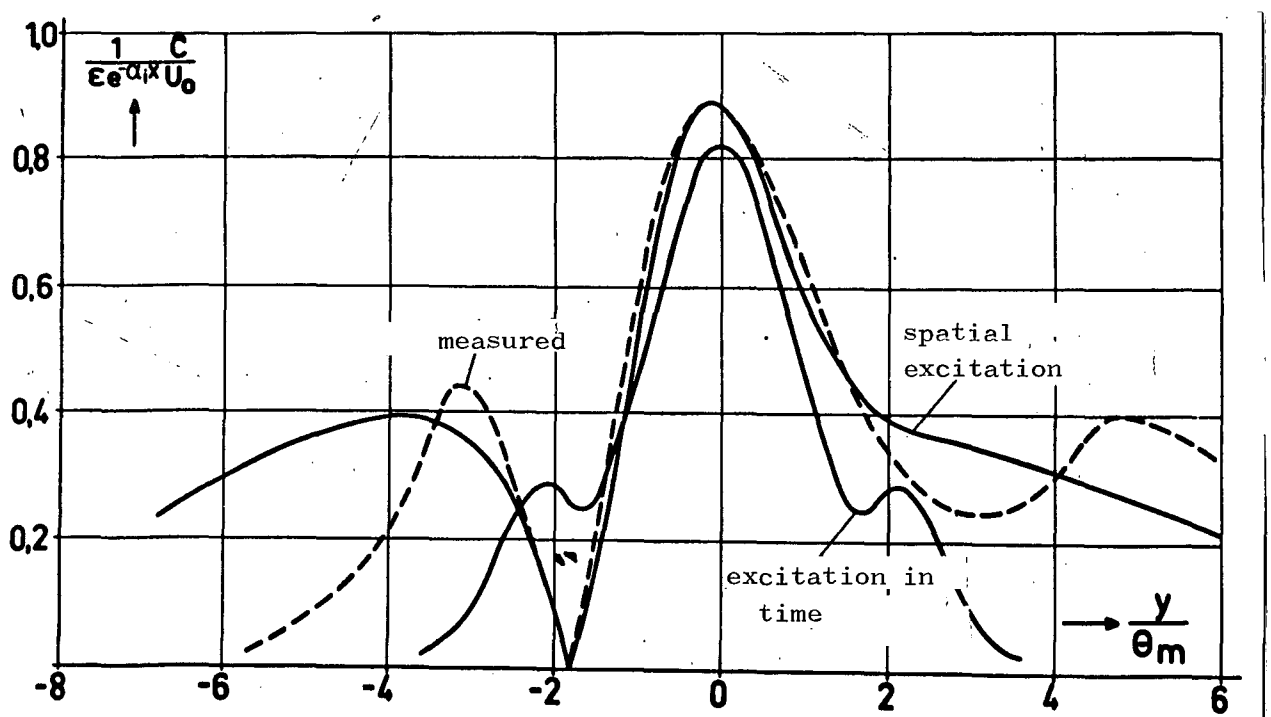

Figure 37. Theoretical and measured amplitude variation at $f \cdot \theta_m / U_o = 0.017$.

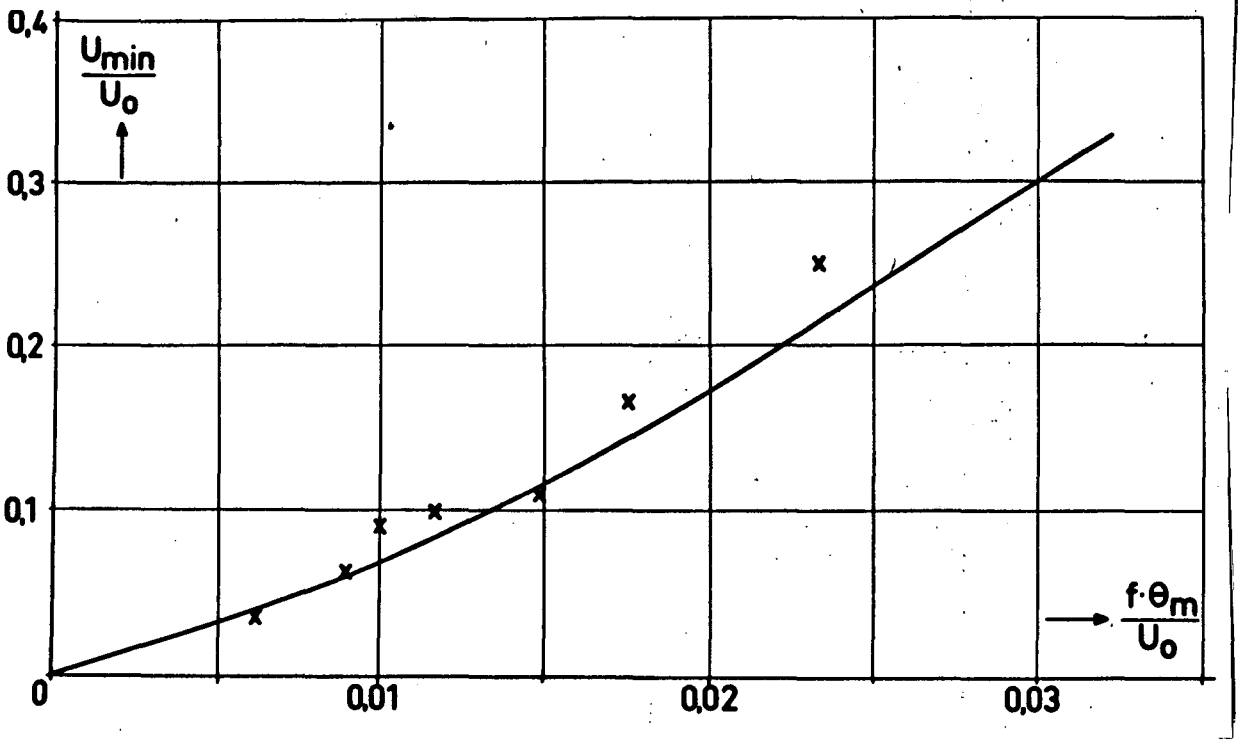

Figure 38. Theoretical and measured dependence of U_{min}/U_O as a function of the Strouhal number.

20

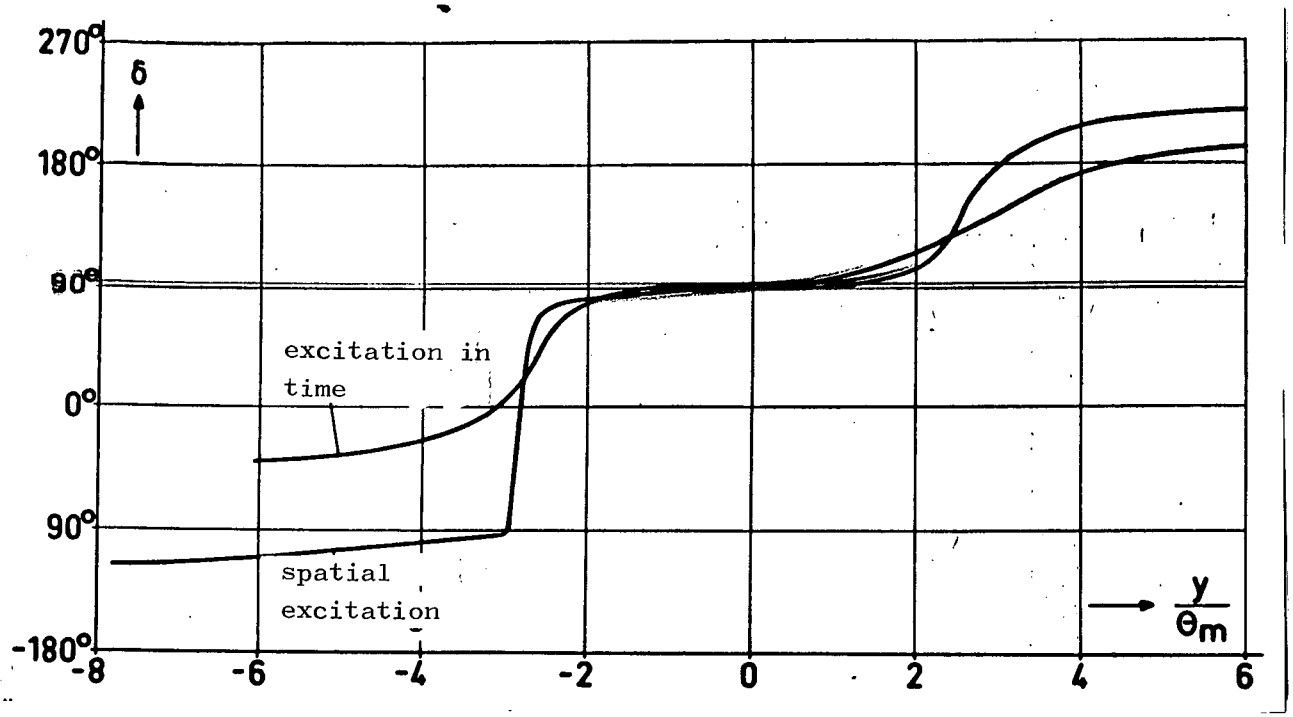

Figure 39. Theoretical phase variation at $f \cdot \theta_m / U_o = 0.008$.

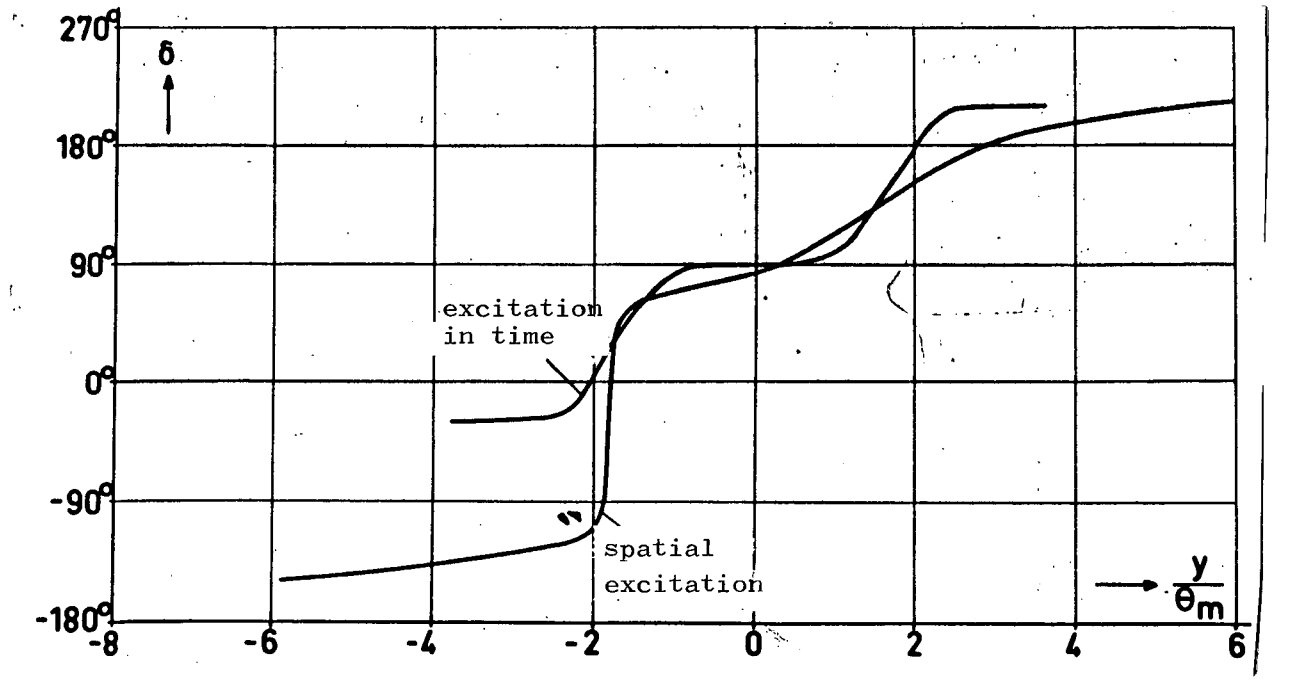

Figure 40. Theoretical phase variation at $f \cdot \theta_m / U_o = 0.017$.

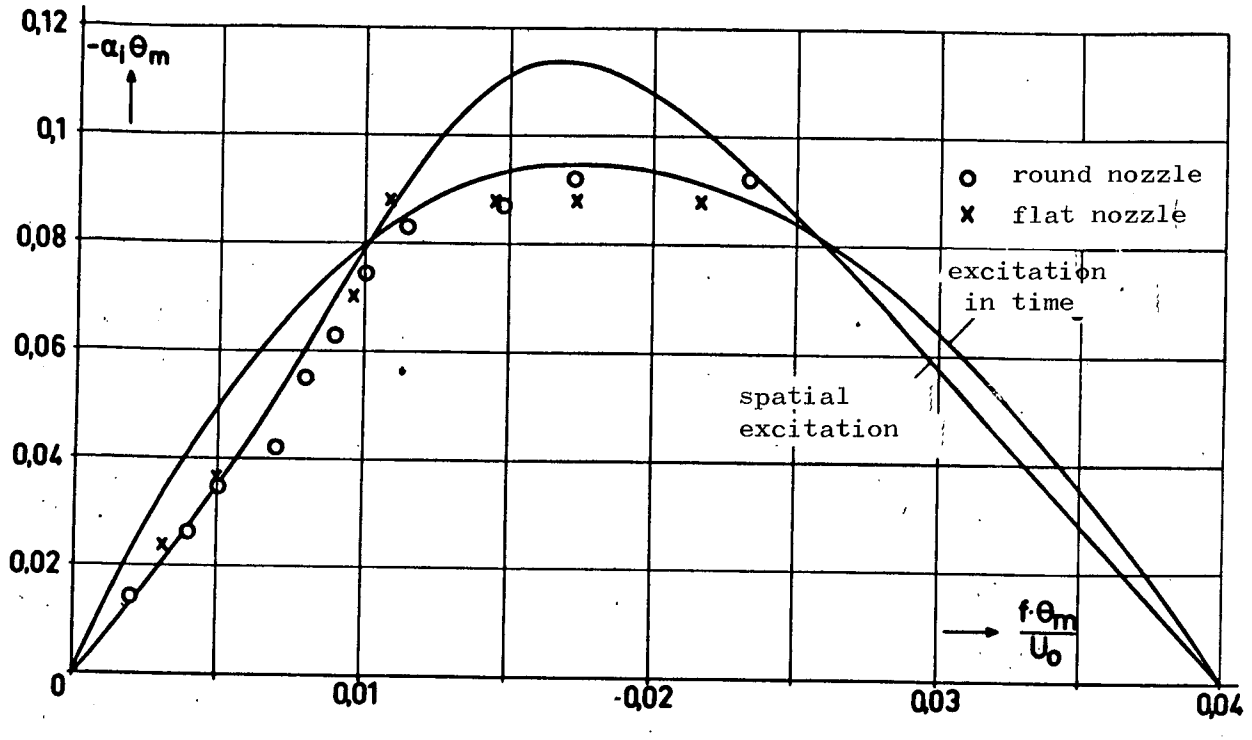

Figure 41. Theoretical and measured excitation factor as a function of the Strouhal number.

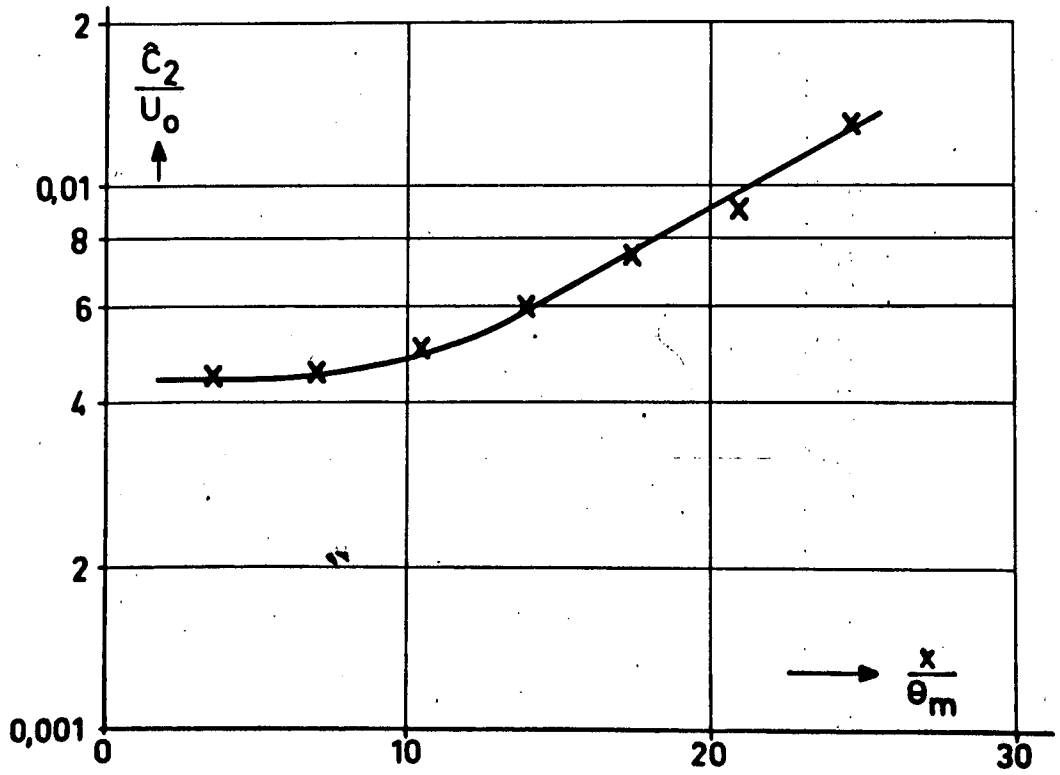

Figure 42. Excitation $\hat{C}_2/U_o$ in the transition range. U_o = 16 m/sec; D = 7.5 cm.

REFERENCES

1. Reynolds, O., "An Experimental Investigation of the Circumstances Which Determine Whether the Motion of Water Shall Be Direct or Sinuous, and of the Law of Resistance in Parallel Channels," Phil. Trans. Roy. Soc., 174, 1883, pp. 935-982. /35

2. Tollmien, W., "The Origin of Turbulence," Report No. 1, Nachr. Ges. Wiss. Gottingen, Math. Klasse, 1929, pp. 21-44.

3. Schlichting, H., "Amplitude Distribution and Energy Balance of Small Turbulences in Plate Flow," Nachr. Ges. Wiss. Gottingen, Math. Phys. Klasse, Fachgruppe, 1, 1, 1935, pp. 47-48.

4. Gortler, H., "The Three-Dimensional Instability of Laminar Boundary Layers at Concave Walls," Nachr. Wiss. Ges. Gottingen, Math. Phys. Klasse, Neue Folge 2, No. 1, 1940.

5. Wille, R., "Flow Phenomena in the Transition Range from Ordered to Random Motion," Jahrbuch d. Schiffbautechn. Ges., 46, 1952, pp. 174-187.

6. Domm, U., "A Hypothesis of the Mechanism of the Origin of Turbulence," DVL-Ber. No. 23, 1956.

7. Wehrmann, O., "Acoustic Control of Turbulent Excitation in Free Jets," Jahrbuch d. WGL, 1957, pp. 102-108.

8. Wille, R., "Growth of Velocity Fluctuations Leading to Turbulence in Free Shear Flow," AFOSR Tech. Rep. Contract AF 61 (052)-412, 1963.

9. Wille, R., Michalke, A., "Flow Phenomena in the Laminar-Turbulent Transition Range of Free Jet Boundary Layers," Verhandl. d. 11. Intern. Kongresses f. Angew. Mech. [Proc., 11th International Congress for Applied Mechanics], Springer, 1964.

10. Wille, R., "Contribution to the Phenomenology of Free Jets," Z. F. Flugwiss., 11, No. 6, 1963, pp. 222-233.

11. Michalke, A., "Vortex Formation in a Free Boundary Layer According to Stability Theory," J. Fluid Mech. 22, part 2, 1964.

12. Timme, A., "Velocity Distribution in Vortices," Ing. Arch., 15, 1957, pp. 205-225.

13. Fabian, H., "Experimental Investigations of Velocity Fluctuations in the Mixing Zone of a Free Jet in the Vicinity of the Nozzle Outlet," DVL-Ber., No. 122, 1960.

14. Schade, H., Michalke, A., "The Formation of Vortices in a Free Boundary Layer," Z. f. Flugwiss. 10, No. 4/5, 1962, pp. 147-154.

15. Michalke, A., Schade, H., "The Stability of Free Boundary Layers," Ing. Arch., 33, 1963, pp. 1-23.

16. Michalke, A., "On the Inviscid Instability of the Hyperbolic-Tangent Velocity Profile," J. Fluid Mech., 19, part 4, 1964, pp. 543-556.

17. Sato, H., "Experimental Investigation on the Transition of a Laminar Separated Layer," J. Phys. Soc. Japan, 11, 1956, pp. 702-709.

18. Berger, E., "Determination of the Hydrodynamic Values of a Karman Vortex Path from Hot Wire Measurements at Small Reynolds Numbers," Z. f. Flugwiss., 12, No. 2, 1964, pp. 41-59.

19. Michalke, A., "Theoretical and Experimental Investigation of a Rotation-Symmetrical Laminar Nozzle Boundary Layer," Ing. Arch., 31, 1962, pp. 268-279.

20. Berger, E., Freymuth, P., Froebel, E., "Application of a Control Technique to the Development of a CT Hot Wire Anemometer," DVL-Ber. No. 282/283, 1963.

21. Brown, G. B., "On Vortex Motion in Gaseous Jets and the Origin of Their Sensitivity to Sound," Proc. Phys. Soc., 47, 1935, pp. 703-732.

22. Bradshaw, P., Ferris, D. H., Johnson, R. F., "Turbulence in the Noise-Producing Region of a Circular Jet," AGARD-Rep., No. 450, 1963.

23. Michalke, A., "Spatially Growing Disturbances in an Inviscid Shear Layer," printed in J. Fluid Mech.

24. Schade, H., "Hydrodynamic Stability Theory of Planar and Axially Symmetric Parallel Flow," DVL-Ber., No. 190, 1962.

Translated for the National Aeronautics and Space Administration under contract No. NASw-2038 by Translation Consultants, Ltd., 944 South Wakefield Street, Arlington, Virginia 22204.